Table 1 Detailed pathological analysis of 31 patients with cerebral amyloid angiopathy

No.	Age	Gender	AD or non-AD	Grade of atherosclerosis at skull base	CAA	SP	NFT	CMI density (/cm^2)				WML
								F	*T*	*P*	*O*	
1	85	M	AD	Moderate	Mild	Frequent	IV	0.00	0.00	0.00	0.00	Mild
2	82	F	AD	Mild	Mild	Frequent	IV	0.00	0.40	–	0.20	Normal
3	76	F	AD	ND	Mild	Frequent	IV	0.51	0.00	0.00	0.00	Moderate
4	86	F	AD	Mild	Mild	Frequent	IV	0.00	0.26	0.47	0.00	Mild
5	80	F	AD	Mild	Mild	Frequent	V	0.45	0.00	0.54	0.00	Moderate
6	67	F	AD	Mild	Mild	Frequent	VI	0.00	0.00	0.31	0.00	Mild
7	84	F	AD	Mild	Mild	Frequent	VI	0.09	0.00	0.00	0.00	Normal
8	68	M	AD	Mild	Moderate	Frequent	IV	0.00	0.00	0.00	0.00	Mild
9	93	F	AD	Moderate	Moderate	Frequent	VI	0.71	0.00	0.00	0.00	Mild
10	84	F	AD	Moderate	Moderate	Frequent	V	0.00	0.26	0.00	0.00	Moderate
11	91	M	AD	Mild	Moderate	Frequent	IV	0.64	0.30	0.55	0.11	Severe
12	85	F	AD	Moderate	Moderate	Frequent	V	1.55	0.55	7.01	0.00	Mild
13	83	M	AD	Normal	Severe	Frequent	IV	12.6	1.49	0.31	2.31	Moderate
14	71	M	AD	Mild	Severe	Frequent	IV	2.00	0.47	4.18	1.58	Mild
15	90	M	Non-AD	Mild	Mild	Sparse	IV	0.00	0.00	0.00	0.00	Moderate
16	66	M	Non-AD	Severe	Mild	Sparse	II	0.00	0.00	0.00	0.29	Normal
17	83	F	Non-AD	Mild	Mild	Sparse	IV	0.00	0.00	0.42	0.00	Moderate
18	84	M	Non-AD	Mild	Mild	Sparse	I	0.00	0.00	0.24	0.00	Mild
19	76	M	Non-AD	Mild	Mild	Sparse	I	0.45	0.00	0.00	0.00	Mild
20	90	F	Non-AD	Mild	Mild	Moderate	IV	0.11	0.00	0.93	0.31	Mild
21	86	M	Non-AD	Mild	Mild	Moderate	IV	0.00	0.24	0.23	0.00	Moderate
22	84	F	Non-AD	Mild	Mild	Moderate	II	0.00	0.00	0.29	0.50	Mild
23	65	M	Non-AD	Normal	Mild	Frequent	V	0.00	0.00	0.00	0.00	Normal
24	81	M	Non-AD	Mild	Mild	Frequent	V	0.20	0.00	0.00	0.00	Moderate
25	72	M	Non-AD	Moderate	Moderate	Sparse	II	0.00	1.45	0.32	0.00	Moderate
26	75	M	Non-AD	Severe	Moderate	Sparse	II	0.19	2.59	1.22	0.33	Mild
27	73	F	Non-AD	Mild	Moderate	Sparse	II	0.19	0.00	0.00	0.00	Mild
28	82	M	Non-AD	Normal	Moderate	Moderate	II	0.49	0.00	0.38	2.17	Mild
29	71	M	Non-AD	Moderate	Severe	None	II	2.55	2.65	3.56	0.94	Mild
30	72	F	Non-AD	Mild	Severe	Sparse	II	2.33	1.10	1.66	6.26	Mild
31	69	F	Non-AD	Mild	Severe	Sparse	III	6.48	8.48	12.8	13.7	Moderate

$p < 0.0001$) (Fig. 4d). This CAA–CMI correlation was observed in all lobes (Fig. 4e); the r value was 0.6377 in the frontal lobe ($p = 0.0014$), 0.5676 in the temporal lobe ($p = 0.0055$), 0.5355 in the parietal lobe ($p = 0.0078$), and 0.5652 in the occipital lobe ($p = 0.0033$). Such CAA–CMI correlation was also observed in both disease groups (AD or non-AD) (Fig. 4f). CMI density was not associated with SP burden ($r = -0.2265$, $p = 0.2204$) (Fig. 4g), or NFT stage ($r = -0.1378$, $p = 0.4597$) (Fig. 4h). Thus, CMI density did not change with greater burden of SP or NFT. CMI density was also not associated with the grade of atherosclerosis ($r = -0.0913$, $p = 0.6312$) (Fig. 4i).

The results of the multivariate analysis are shown in Table 3. The severity of CAA was a significant multivariate predictor ($p = 0.0022$), with a standard partial regression coefficient of 0.6395. Similar trends were evident in each lobe (frontal, $p = 0.0014$; temporal, $p = 0.0055$; parietal, $p = 0.0078$; occipital, $p = 0.0033$). However, age ($p = 0.5979$), the grade of atherosclerosis ($p = 0.3973$), AD or non-AD ($p = 0.8364$), SP burden ($p = 0.5164$), NFT stage ($p = 0.3870$), or the grade of WML ($p = 0.6931$) were not significant multivariate predictors.

Cerebral blood flow in mice after BCAS

The BCAS operation reduced CBF by 15% in 20-week-old wild-type mice and 26% in Tg-SwDI mice of the same age after 12 weeks with a statistically significant difference ($p = 0.0412$) (Supplementary Fig. 3).

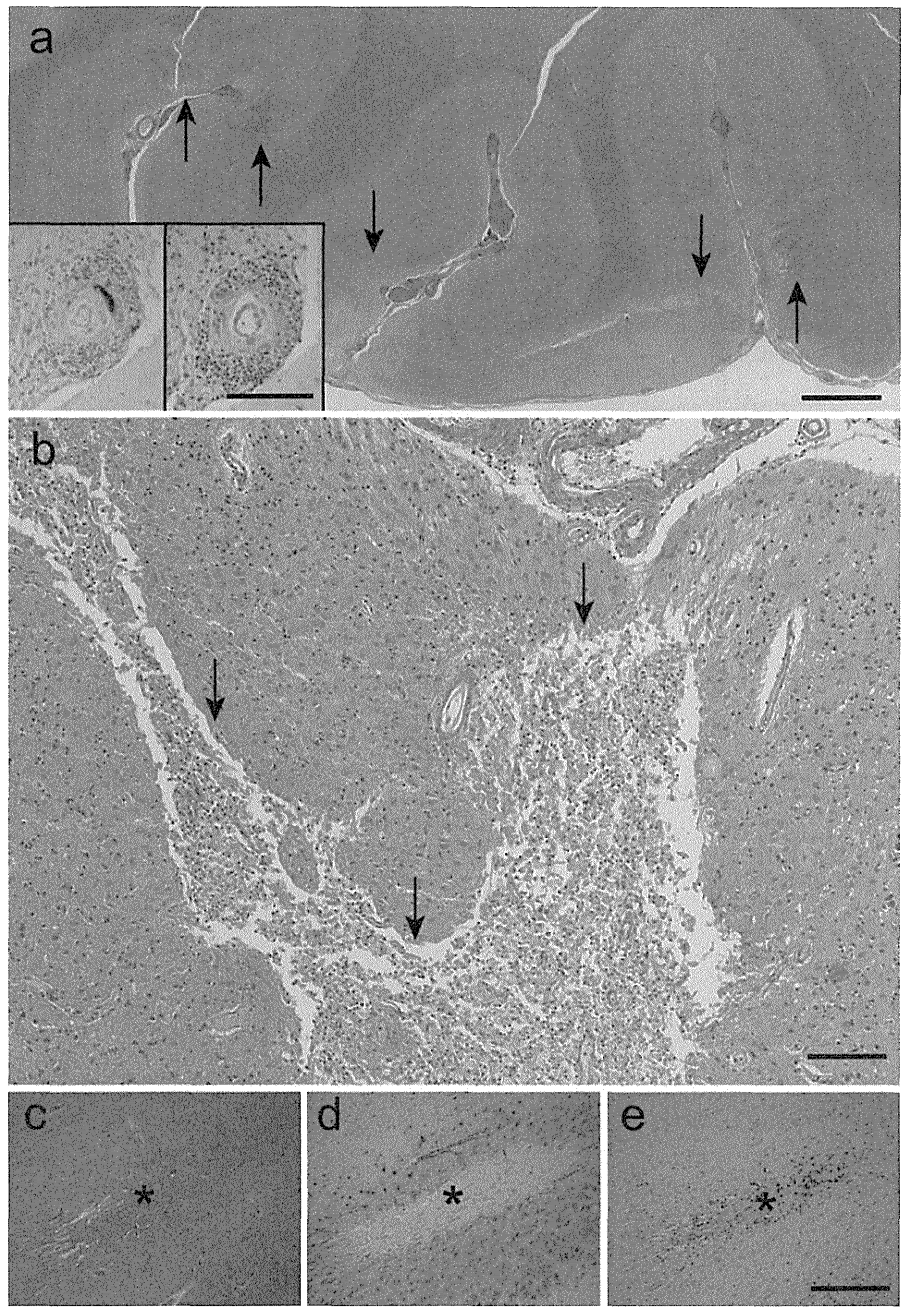

Fig. 2 Representative photomicrographs of CMIs from patients with CAA. **a** CMIs (*arrows*) were present in the temporal cortex in a patient with CAA-related inflammation (H&E staining). Vascular Aβ depositions (*brown*) and marked vascular/perivascular infiltration of inflammatory cells are shown in insets (*left*, anti-Aβ immunostaining with hematoxylin counterstain; right, H&E staining). **b**, A CMI (*arrows*) in the occipital cortex in a patient with AD. **c–e** A CMI was accompanied with GFAP-positive reactive astroglial cells and CD68-positive macrophage/microglial proliferation (adjacent sections; **c** H&E; **d** GFAP; and **e** CD68). *Bars* indicate 300 μm in **a**, 50 μm in **b**, and 100 μm in **c–e** and insets in **a**

Histological findings in Tg-SwDI mice

We found that microinfarcts developed in a subset of BCAS-operated Tg-SwDI mice (Fig. 5). The percentage of BCAS-operated Tg-SwDI mice ($n = 17$) exhibiting microinfarcts was 33.3 (2 out of 6), 42.9 (3 out of 7) and 25.0% (1 out of 4) at 18, 24, and 32 weeks of age. However, microinfarcts were not found in sham-operated Tg-SwDI mice ($n = 14$) or BCAS-operated wild-type mice ($n = 15$) up to 32 weeks of age. The number of microinfarcts in BCAS-operated Tg-SwDI mice, sham-operated Tg-SwDI mice, and BCAS-operated wild-type mouse was listed in Supplementary Table 3. Immunohistochemical analysis showed that ischemic insults accelerated perivascular and leptomeningeal Aβ accumulations (Fig. 6a, b). Generally, the immunostained patterns of $A\beta_{1-40}$ and $A\beta_{1-42}$ were quite similar, although Aβ40 immunostaining was more intense than $A\beta_{1-42}$, in accordance with a previous biochemical study [11]. Aβ accumulation was evident in and around microvessels as well as larger cerebral vessels (approximately 10–15 μm in diameter), in the leptomeningeal arteries of BCAS-operated Tg-SwDI mice at

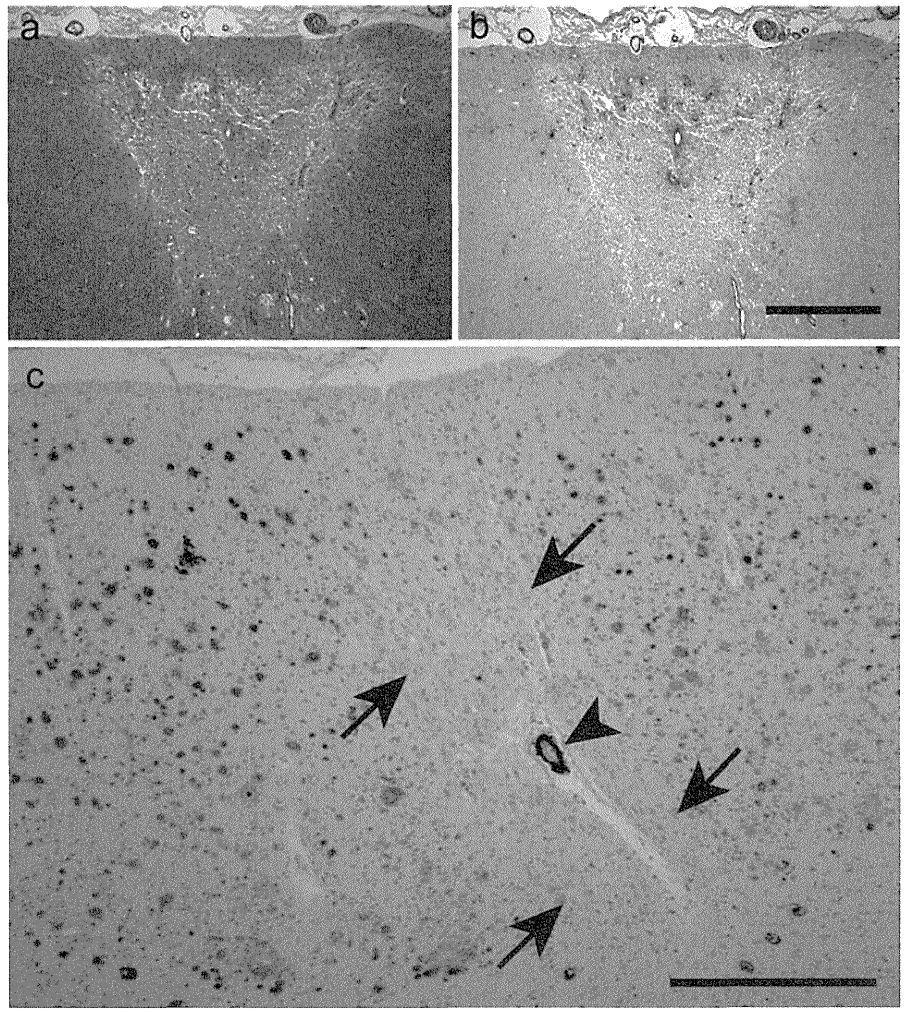

Fig. 3 Representative photomicrographs of CMIs stained with H&E and Aβ from patients with CAA. **a**, **b** CMIs were located in close proximity to Aβ-deposited vessels. **a** and **b** are adjacent sections (**a** H&E; **b** Aβ). **c** Aβ-positive senile plaques were not apparent inside a CMI (*arrows*). The *arrowhead* indicates an Aβ-positive arteriole within a CMI. *Bars* indicate 500 μm in **a** and **b**, and 100 μm in **c**

18 weeks of age; however, Aβ accumulation in the leptomeningeal arteries were less apparent in sham-operated Tg-SwDI mice at 18 or 24 weeks of age (Fig. 6b). As a result, two-way ANOVA showed that BCAS had a significant [F (1, 25) = 18.5, $p = 0.0002$] effect on leptomeningeal Aβ accumulation. However, there was no effect of age on leptomeningeal Aβ accumulation [F (2, 25) = 1.73, $p = 0.20$] (Fig. 6f), suggesting a ceiling effect of age on leptomeningeal Aβ accumulation.

By contrast, in the hippocampus and the cerebral cortex, two-way ANOVA showed a significant effect of age [hippocampus, F (2, 25) = 15.8, $p < 0.0001$; cortex, F (2, 25) = 7.02, $p = 0.0038$] but no effect of the operation [hippocampus, F (1, 25) = 2.79, $p = 0.11$; cortex, F (1, 25) = 0.73, $p = 0.40$] on Aβ accumulation (Fig. 6a, d, e).

In all Tg-SwDI mice combined, the amount of leptomeningeal Aβ was significantly greater in mice with microinfarcts (3.4-fold), compared to those without microinfarcts ($p = 0.0004$). Most microinfarcts were seen in the cortex (Fig. 5b) and close to the Aβ-deposited vessels; however, some microinfarcts were also seen in the hippocampus CA1 area in the 18, 24, and 32-week-old BCAS-operated Tg-SwDI mice (Fig. 5d). A small number of microhemorrhages were also detected in the ventral part of the thalamus in the 32-week-old BCAS-operated Tg-SwDI mice (Fig. 5e, f), although such changes were not found in sham-operated Tg-SwDI mice or BCAS-operated wild-type mice up to 32 weeks of age (Fig. 5a, c). Thrombus formation was not apparent in any sections assessed.

Discussion

We found that CMI density is related to CAA severity, but not to SP or NFT burden severity, suggesting that the presence of Aβ causes loss of vascular autoregulation associated with rigidity of arterioles, leading to infarction in the territory of their branching vessels. Thrombus formation induced by endothelial damage in CAA may have also been involved in the CMI development although the thrombus

Table 2 Univariate analysis of variables

Factors	*N*	CMI density	*r* value	*p* value
Age (years)			−0.2570	0.1627
<70	5	2.101		
70–79	8	1.142		
80–89	18	0.520		
Atherosclerosis			−0.0913	0.6312
Normal (0)	3	1.642		
Mild (1)	19	0.916		
Moderate (2)	6	0.898		
Severe (3)	2	0.578		
Disease			−0.1007	0.5900
Non-AD (0)	17	1.118		
AD (1)	14	0.714		
CAA			0.6736	<0.0001
Mild (1)	17	0.112		
Moderate (2)	9	0.584		
Severe (3)	5	4.368		
SP			−0.2265	0.2204
None (0)	1	2.425		
Sparse (1)	10	1.511		
Moderate (2)	4	0.353		
Frequent (3)	16	0.628		
NFT			−0.1378	0.4597
I (1)	2	0.086		
II (2)	8	0.983		
III (3)	1	10.353		
IV (4)	12	0.641		
V (5)	5	0.528		
VI (6)	3	0.093		
WML			0.1962	0.2902
Normal (0)	4	0.074		
Mild (1)	16	0.790		
Moderate (2)	10	1.567		
Severe (3)	1	0.400		

was found only in one patient with CAA but not in any Tg-SwDI mice. The severity of white matter changes was not associated with the CMI density, which may raise the possibility that the CMIs and white matter changes have different formation processes as white matter damage is reported to reflect a progressive microangiopathy due to CAA [10]. Furthermore, our study showed that CMI density is no greater in AD than in other disorders accompanied with CAA. Given that CMI is also a strong determinant for dementia [23, 49], the observed correlation between CMI and CAA strengthens the notion that, although underestimated, these two pathologies are important substrates of cognitive decline in the elderly [15, 16].

Previous studies have reported an association between CMI and CAA in AD [15, 16, 34, 40], but others have found no such link [12, 24]. Inconsistencies between different studies might be attributable to the heterogeneity of underlying vascular pathology in AD as cerebrovascular changes can occur concomitantly with AD pathology, and also because CAA may contribute to the development of various types of cerebrovascular diseases such as lobar hemorrhage, microbleeds, and white matter lesions [39]. The issue is further complicated by the fact that CAA usually accompanies AD, but does not exclusively result from AD. Thus, accordingly, a significant correlation has been reported between the severity of CAA and the amount of CMIs in only one other study using postmortem brains of vascular dementia [16]. The current study, which used an unbiased collection of brains including non-AD samples, confirms the previous report and suggests that CAA along with chronic cerebral hypoperfusion may give rise to CMIs, which appear to be true substrates of cognitive impairment [14]. This may explain the previous findings, which have indicated that severity of CAA is associated with increased frequency of antemortem cognitive decline [25, 31]. Our findings, which show a strong association between CMIs and CAA, are supported by additional animal studies using the Tg-SwDI mice subjected to chronic cerebral hypoperfusion; when combined these findings have demonstrated that cerebral hypoperfusion induces: (1) accumulation of CAA-like vascular Aβ and resultant vascular compromise and (2) development of microinfarcts and even microhemorrhages in a subset of animals. Since microinfarcts did not develop in wild-type mice after BCAS, the data suggest that both CAA and hypoperfusion are required for microinfarct development. Tg-SwDI mice may have morphological changes in the endothelium and in the basement membranes of capillaries and arteries, leading to a failure of the mechanisms of clearance of Aβ and other metabolites. Hypoperfusion may interfere with the arterial pulsations and with the interstitial fluid pressure, leading to reduced perivascular clearance of Aβ as manifested by CAA associated with microinfarcts.

We have previously shown that chronic cerebral hypoperfusion increased the amount of filter-trap Aβ in the extracellular-enriched soluble brain fraction of mice overexpressing a mutant form of the human APP [22, 51]; in this mouse model exhibiting senile plaques, the neuronal loss and cognitive impairment that were both accelerated by hypoperfusion was explained by the disturbed Aβ metabolism. In the current study using mice overexpressing vasculotropic mutant Aβ, the hypoperfusion-induced aggravation of CAA may then result from increased synthesis of Aβ [45]. Alternatively, cerebral hypoperfusion and reduced vascular pulsation may impede clearance of Aβ as it is hypothesized that motive force of vessel pulsation is required for perivascular clearance of interstitial fluid containing Aβ [47]. This mechanism may temporarily

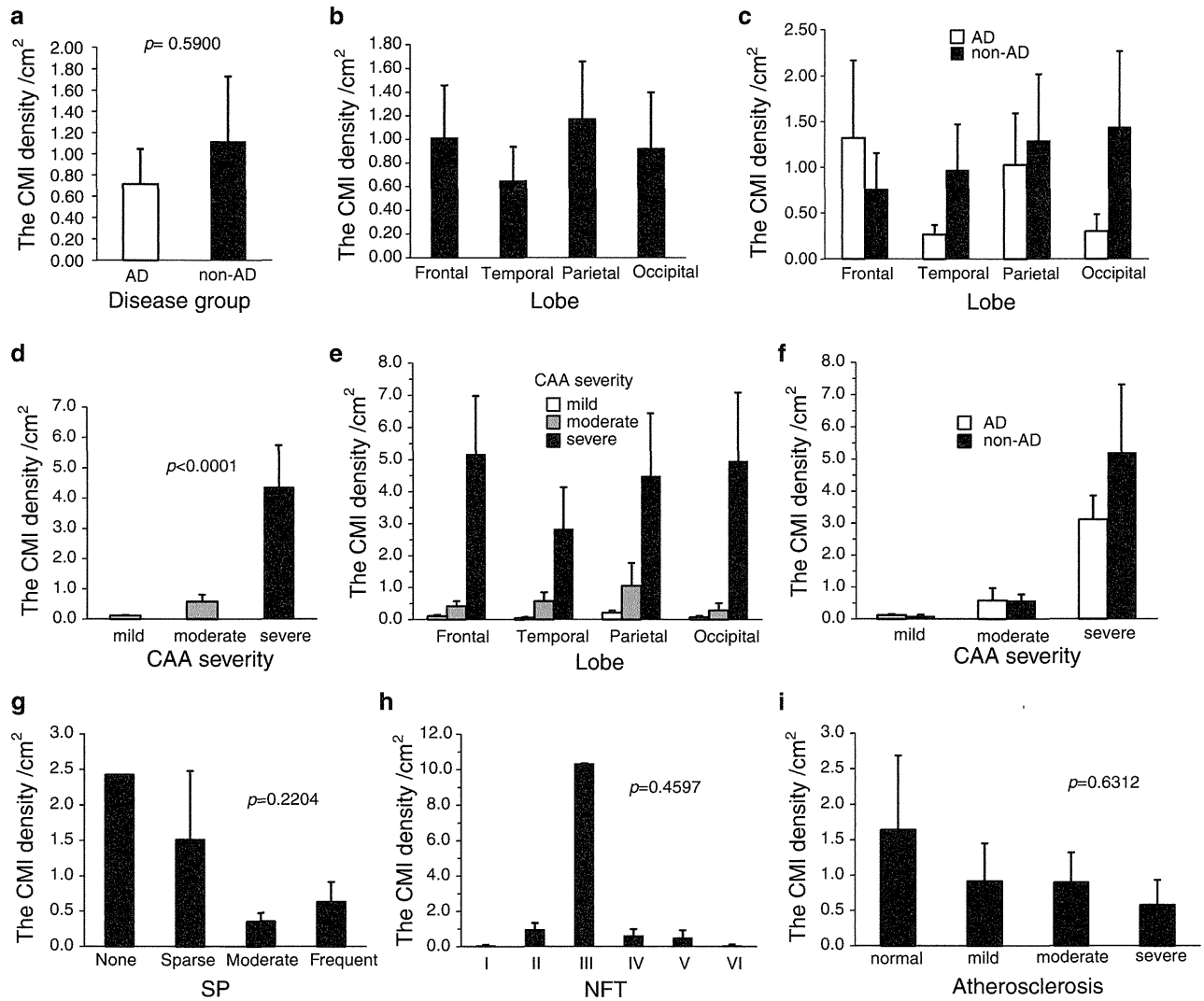

Fig. 4 Correlation of CMI density with CAA severity. **a** A diagram showing no significant difference in CMI density between AD and non-AD groups (*$p = 0.5900$). **b** A diagram showing CMI density in each lobe of AD and non-AD groups combined. **c** Diagram showing CMI density in each lobe of AD and non-AD groups. **d** Significant correlation of CMI density with CAA severity (*$p < 0.0001$). **e** CAA-CMI correlation was observed in each lobe. **f** CAA–CMI correlation was observed in both AD and non-AD group. **g** CMI density was not associated with SP burden (*$p = 0.2204$). **h** CMI density was not associated with NFT stage (*$p = 0.4597$). **i** CMI density was not associated with atherosclerosis grade (*$p = 0.6312$)

Table 3 Multivariate analysis of variables

Variables	Partial regression coefficient	Standard partial regression coefficient	*t* value	*p* value	Tolerance
CAA severity	1.7190	0.6395	3.4654	0.0022	0.4220
NFT stage	0.3019	0.2168	0.8825	0.3870	0.3555
Atherosclerosis grade	−0.4188	−0.1483	−0.8632	0.3973	0.7284
SP burden	−0.4848	−0.2346	−0.6596	0.5164	0.1723
Age	−0.0244	−0.0968	−0.5352	0.5979	0.6704
WML grade	0.1970	0.0698	0.3999	0.6931	0.7247
Disease	−0.2555	−0.0626	−0.2090	0.8364	0.2468

aggravate CAA, which may compromise cerebral perfusion and ultimately lead to development of microinfarcts. Thus, the impaired microvascular function observed may impede perivascular drainage pathway of Aβ, forming a cycle of vascular Aβ deposition.

Our findings may also have implications in the understanding of the pathological complications of Aβ immunotherapy. The hypoperfusion-induced abnormalities seen in Tg-SwDI mice may be similar to the findings in AD patients who have received Aβ immunotherapy; in immunized AD group, microvascular lesions, such as CMIs or microhemorrhages, occurred with a higher density than non-immunized AD control group; this may have been because soluble Aβ mobilized from the amyloid deposits had not cleared efficiently from AD brains [6, 35]. It is plausible that the aging- and AD-associated microvascular changes [18] cannot cope with overwhelming amount of Aβ mobilized from the Aβ deposits at least partially due to existing reduction of vessel pulsation and/or hypoperfusion, leading to formation of CMIs or microhemorrhages in immunized AD patients. The current study indicates that such mechanisms underlie the formation of CMIs, even in

Fig. 6 Enhanced Aβ deposition in Tg-SwDI mice after cerebral hypoperfusion. **a** Aβ immunohistochemical staining showing that following cerebral hypoperfusion, Tg-SwDI mice exhibited cortical Aβ deposition at 24 weeks of age (*right middle panel*) and more extensively at 32 weeks of age (*right lower panel*). Sham-operated Tg-SwDI mice showed cortical Aβ deposition at 32 weeks of age (*left lower panel*). Insets show representative images of vascular and perivascular Aβ deposition. **b** Aβ immunohistochemical staining showing that following cerebral hypoperfusion, Tg-SwDI mice exhibited Aβ deposition in the leptomeninges containing leptomeningeal arteries (*arrows*) at 18 weeks of age (*right upper panel*) and more extensively at 24 and 32 weeks of age (*right middle* and *lower panels*), although sham-operated Tg-SwDI mice began to show such changes at 32 weeks of age (*left lower panel*). Insets show representative images of vascular and perivascular Aβ deposition in the leptomeningeal artery. In **a** and **b**, the mouse anti-$Aβ_{1–40}$ (BA27) antibody was used. **c** The schematic illustration of the regions of interest depicted in the cerebral cortex (size, 500 × 300 μm each), the hippocampus (500 × 300 μm each), and the leptomeninges including the pia and arteries (300 × 50 μm each) of the parasagittal section of the brain. **d–f** Densitometric analyses of temporal profiles of Aβ depositions in the cerebral cortex (**d**), the hippocampus (**e**), and the leptomeninges (**f**). Leptomeningeal vascular, as well as pial, Aβ accumulation was jointly analyzed as 'leptomeningeal Aβ'. There seems to be a ceiling effect of age on leptomeningeal Aβ accumulation. *CPu* caudoputamen, *Cx* cortex, *Hip* hippocampus, *LM* leptomeninge, *LV* lateral ventricle, *Thal* thalamus. *Bars* indicate 40 μm in **a** and **b** and 8 μm in insets in **a** and **b**

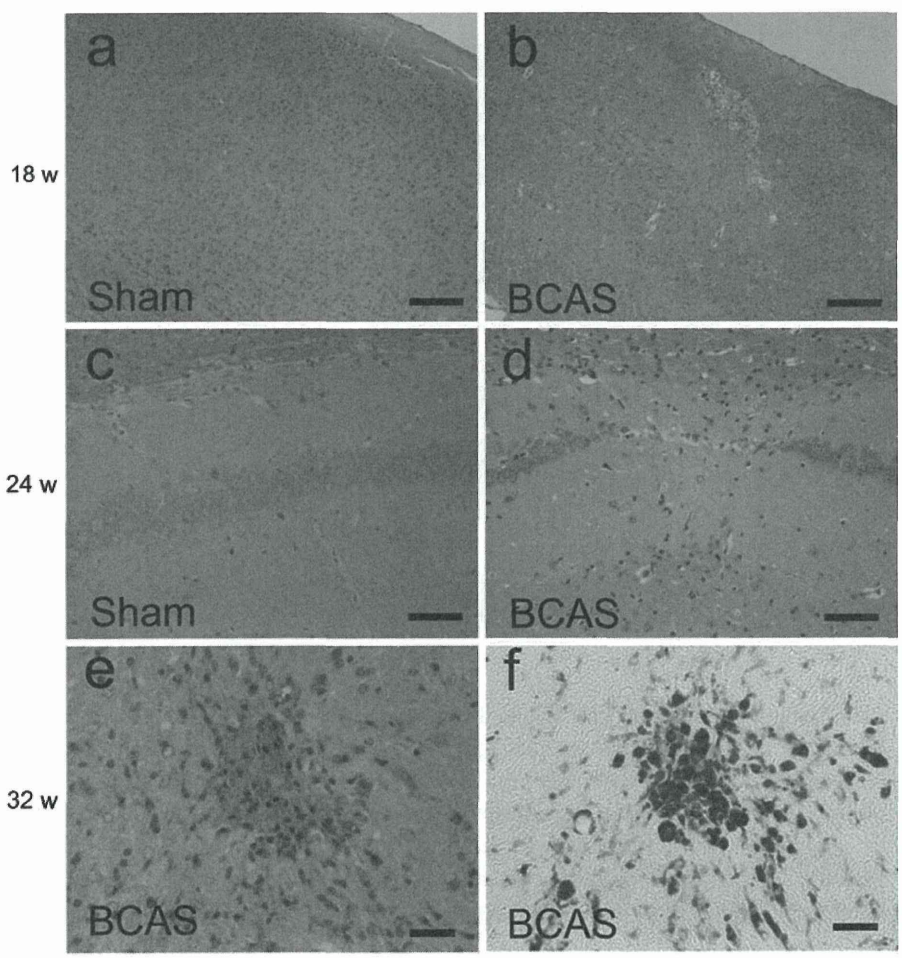

Fig. 5 Appearance of microinfarcts and microhemorrhages in Tg-SwDI mice after cerebral hypoperfusion. **a–e** Representative photomicrographs of H&E staining showing that following BCAS-induced cerebral hypoperfusion, a cortical microinfarct developed at 18 weeks of age in three of six Tg-SwDI mice (**b**), a hippocampal microinfarct at 24 weeks of age in three of seven Tg-SwDI mice (**d**), and a striatal microhemorrhage at 32 weeks of age in one of four Tg-SwDI mice (**e**), although such changes were not found in sham-operated Tg-SwDI mice at indicated time points (**a**, **c**). **f** Perls-Stieda's iron staining showing the striatal microhemorrhage. *Bars* indicate 200 μm in **a–d** and 40 μm in **e** and **f**

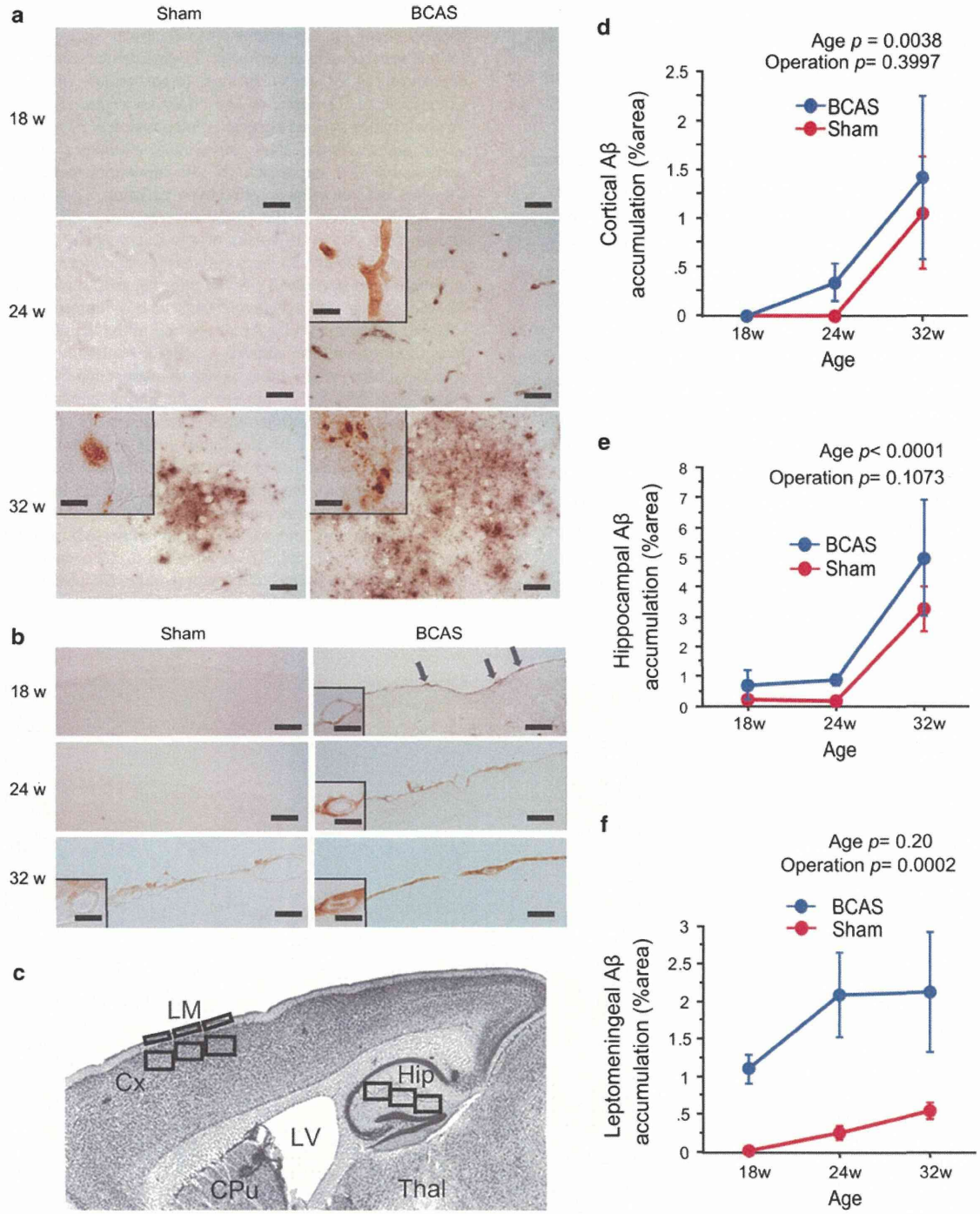

non-immunized patients with CAA. The degree of hypoperfusion and microvascular changes may predict the response rate of Aβ immunotherapy and the emergence rate of ischemic complications. However, it remains to be determined whether chronic cerebral hypoperfusion hampers the Aβ drainage pathway directly through reduced arterial pulsation or indirectly through upregulated Aβ synthesis.

The main limitation of this study is the lack of clinical and neuropsychometric information on the postmortem brains used. This meant that we could not directly relate our pathological findings to antemortem hypoperfusive and cognitive status. Another limitation is that CAA or CMI severity could not be related to the apolipoprotein E genotype [36], due to ethical and legal constraints of genotype extraction. In addition, the use of the CERAD

criteria for assessing the burden of neuritic plaques and the Braak staging for the burden of NFTs both based on the modified Bielschowsky staining may be the third limitation, considering that the CERAD is semiquantitative rather than quantitative measures of neuropathology [28] and the Braak staging criteria for tau pathology have been recently modified [2], although the two neuropathologists agreed on their final grading of the 31 CAA patients enrolled in the current study.

In summary, using postmortem brain analysis of relevant patients and models of transgenic mice, our study provides strong evidence for the relationship between CAA and microinfarcts with cerebral hypoperfusion as the mediating factor. Our observations support the notion that CAA is one of the pathological substrates that links neurodegenerative and vascular processes.

Acknowledgments We would like to express our cordial gratitude to Ms. Takako Kawada and Ms. Mayumi Ohara for their excellent technical assistance, and Dr. Ahmad Khundakar for his critical reading of the manuscript. We gratefully acknowledge grant support from the Lifelong Health & Wellbeing programme supported by the Research Councils UK Newcastle Centre for Brain Ageing and Vitality (R.N.K.), Alzheimer's Research UK (R.N.K.), the UK NIHR Biomedical Research Centre for Ageing and Age Related Diseases award to the Newcastle upon Tyne Hospitals NHS Foundation Trust (R.N.K.), the Bayer Scholarship for Cardiovascular Research (M.I.), the Univers Foundation (M.I.), and the Grants-in-Aid for Scientific Research (B) (M.I. No. 23390233).

Conflict of interest The authors have no conflict of interest to declare.

Open Access This article is distributed under the terms of the Creative Commons Attribution Noncommercial License which permits any noncommercial use, distribution, and reproduction in any medium, provided the original author(s) and source are credited.

References

1. Akiguchi I, Tomimoto H, Suenaga T, Wakita H, Budka H (1998) Blood–brain barrier dysfunction in Binswanger's disease; an immunohistochemical study. Acta Neuropathol 95:78–84
2. Alafuzoff I, Arzberger T, Al-Sarraj S et al (2008) Staging of neurofibrillary pathology in Alzheimer's disease: a study of the BrainNet Europe Consortium. Brain Pathol 18:484–496
3. American Psychiatric Association (1994) Diagnostic and statistical manual of mental disorders, 4th edn. American Psychiatric Press, Washington, DC
4. Attems J, Jellinger K, Thal DR, Van Nostrand W (2011) Review: sporadic cerebral amyloid angiopathy. Neuropathol Appl Neurobiol 37:75–93
5. Bennett DA, Wilson RS, Gilley DW, Fox JH (1990) Clinical diagnosis of Binswanger's disease. J Neurol Neurosurg Psychiatry 53:961–965
6. Boche D, Zotova E, Weller RO et al (2008) Consequence of Abeta immunization on the vasculature of human Alzheimer's disease brain. Brain 131:3299–3310
7. Braak H, Braak E (1991) Neuropathological stageing of Alzheimer-related changes. Acta Neuropathol 82:239–259
8. Braak H, Alafuzoff I, Arzberger T, Kretzschmar H, Del Tredici K (2006) Staging of Alzheimer disease-associated neurofibrillary pathology using paraffin sections and immunocytochemistry. Acta Neuropathol 112:389–404
9. Brun A, Englund E (1986) A white matter disorder in dementia of the Alzheimer type: a pathoanatomical study. Ann Neurol 19: 253–262
10. Chen YW, Gurol ME, Rosand J et al (2006) Progression of white matter lesions and hemorrhages in cerebral amyloid angiopathy. Neurology 67:83–87
11. Davis J, Xu F, Deane R et al (2004) Early-onset and robust cerebral microvascular accumulation of amyloid beta-protein in transgenic mice expressing low levels of a vasculotropic Dutch/Iowa mutant form of amyloid beta-protein precursor. J Biol Chem 279:20296–20306
12. Ellis RJ, Olichney JM, Thal LJ et al (1996) Cerebral amyloid angiopathy in the brains of patients with Alzheimer's disease: the CERAD experience, part XV. Neurology 46:1592–1596
13. Grinberg LT, Thal DR (2010) Vascular pathology in the aged human brain. Acta Neuropathol 119:277–290
14. Hachinski V, Iadecola C, Petersen RC et al (2006) National Institute of Neurological Disorders and Stroke–Canadian Stroke Network vascular cognitive impairment harmonization standards. Stroke 37:2220–2241
15. Haglund M, Sjobeck M, Englund E (2004) Severe cerebral amyloid angiopathy characterizes an underestimated variant of vascular dementia. Dement Geriatr Cogn Disord 18: 132–137
16. Haglund M, Passant U, Sjobeck M, Ghebremedhin E, Englund E (2006) Cerebral amyloid angiopathy and cortical microinfarcts as putative substrates of vascular dementia. Int J Geriatr Psychiatry 21:681–687
17. Ihara M, Polvikoski TM, Hall R et al (2010) Quantification of myelin loss in frontal lobe white matter in vascular dementia, Alzheimer's disease, and dementia with Lewy bodies. Acta Neuropathol 119:579–589
18. Kalaria RN (1996) Cerebral vessels in ageing and Alzheimer's disease. Pharmacol Ther 72:193–214
19. Kalaria RN, Kenny RA, Ballard CG, Perry R, Ince P, Polvikoski T (2004) Towards defining the neuropathological substrates of vascular dementia. J Neurol Sci 226:75–80
20. Kalaria RN, Thomas A, Oakley A et al (2003) Cerebrovascular amyloidosis and dementia. Curr Med Chem Immunol Endocr Metab Agents 3:317–327
21. Kawamoto Y, Akiguchi I, Nakamura S, Budka H (2002) Accumulation of 14-3-3 proteins in glial cytoplasmic inclusions in multiple system atrophy. Ann Neurol 52:722–731
22. Kitaguchi H, Tomimoto H, Ihara M et al (2009) Chronic cerebral hypoperfusion accelerates amyloid beta deposition in APPSwInd transgenic mice. Brain Res 1294:202–210
23. Kovari E, Gold G, Herrmann FR et al (2004) Cortical microinfarcts and demyelination significantly affect cognition in brain aging. Stroke 35:410–414
24. Launer LJ, Petrovitch H, Ross GW, Markesbery W, White LR (2008) AD brain pathology: vascular origins? Results from the HAAS autopsy study. Neurobiol Aging 29:1587–1590
25. Matthews FE, Brayne C, Lowe J, McKeith I, Wharton SB, Ince P (2009) Epidemiological pathology of dementia: attributable-risks at death in the Medical Research Council Cognitive Function and Ageing Study. PLoS Med 6:e1000180
26. McCarran WJ, Goldberg MP (2007) White matter axon vulnerability to AMPA/kainate receptor-mediated ischemic injury is developmentally regulated. J Neurosci 27:4220–4229
27. McKeith IG, Dickson DW, Lowe J et al (2005) Diagnosis and management of dementia with Lewy bodies: third report of the DLB Consortium. Neurology 65:1863–1872

28. Mirra SS, Gearing M, McKeel DW Jr et al (1994) Interlaboratory comparison of neuropathology assessments in Alzheimer's disease: a study of the Consortium to Establish a Registry for Alzheimer's Disease (CERAD). J Neuropathol Exp Neurol 53: 303–315
29. Mirra SS, Heyman A, McKeel D et al (1991) The Consortium to Establish a Registry for Alzheimer's Disease (CERAD). Part II. Standardization of the neuropathologic assessment of Alzheimer's disease. Neurology 41:479–486
30. Nakaji K, Ihara M, Takahashi C et al (2006) Matrix metalloproteinase-2 plays a critical role in the pathogenesis of white matter lesions after chronic cerebral hypoperfusion in rodents. Stroke 37:2816–2823
31. Neuropathology Group. Medical Research Council Cognitive Function Aging Study (2001) Pathological correlates of late-onset dementia in a multicentre, community-based population in England and Wales. Neuropathology Group of the Medical Research Council Cognitive Function and Ageing Study (MRC CFAS). Lancet 357:169–175
32. Nishio K, Ihara M, Yamasaki N et al (2010) A mouse model characterizing features of vascular dementia with hippocampal atrophy. Stroke 41:1278–1284
33. Okamoto Y, Ihara M, Fujita Y, Ito H, Takahashi R, Tomimoto H (2009) Cortical microinfarcts in Alzheimer's disease and subcortical vascular dementia. Neuroreport 20:990–996
34. Olichney JM, Hansen LA, Hofstetter CR, Grundman M, Katzman R, Thal LJ (1995) Cerebral infarction in Alzheimer's disease is associated with severe amyloid angiopathy and hypertension. Arch Neurol 52:702–708
35. Patton RL, Kalback WM, Esh CL et al (2006) Amyloid-beta peptide remnants in AN-1792-immunized Alzheimer's disease patients: a biochemical analysis. Am J Pathol 169:1048–1063
36. Premkumar DR, Cohen DL, Hedera P, Friedland RP, Kalaria RN (1996) Apolipoprotein E-epsilon4 alleles in cerebral amyloid angiopathy and cerebrovascular pathology associated with Alzheimer's disease. Am J Pathol 148:2083–2095
37. Shibata M, Ohtani R, Ihara M, Tomimoto H (2004) White matter lesions and glial activation in a novel mouse model of chronic cerebral hypoperfusion. Stroke 35:2598–2603
38. Shibata M, Yamasaki N, Miyakawa T et al (2007) Selective impairment of working memory in a mouse model of chronic cerebral hypoperfusion. Stroke 38:2826–2832
39. Smith EE, Greenberg SM (2009) Beta-amyloid, blood vessels, and brain function. Stroke 40:2601–2606
40. Soontornniyomkij V, Lynch MD, Mermash S et al (2010) Cerebral microinfarcts associated with severe cerebral beta-amyloid angiopathy. Brain Pathol 20:459–467
41. Suter OC, Sunthorn T, Kraftsik R et al (2002) Cerebral hypoperfusion generates cortical watershed microinfarcts in Alzheimer disease. Stroke 33:1986–1992
42. Thal DR, Griffin WS, de Vos RA, Ghebremedhin E (2008) Cerebral amyloid angiopathy and its relationship to Alzheimer's disease. Acta Neuropathol 115:599–609
43. Underhill SM, Goldberg MP (2007) Hypoxic injury of isolated axons is independent of ionotropic glutamate receptors. Neurobiol Dis 25:284–290
44. Vonsattel JP, Myers RH, Hedley-Whyte ET, Ropper AH, Bird ED, Richardson EP Jr (1991) Cerebral amyloid angiopathy without and with cerebral hemorrhages: a comparative histological study. Ann Neurol 30:637–649
45. Wang Z, Wu D, Vinters HV (2002) Hypoxia and reoxygenation of brain microvascular smooth muscle cells in vitro: cellular responses and expression of cerebral amyloid angiopathy-associated proteins. APMIS 110:423–434
46. Weller RO, Boche D, Nicoll JA (2009) Microvasculature changes and cerebral amyloid angiopathy in Alzheimer's disease and their potential impact on therapy. Acta Neuropathol 118:87–102
47. Weller RO, Djuanda E, Yow HY, Carare RO (2009) Lymphatic drainage of the brain and the pathophysiology of neurological disease. Acta Neuropathol 117:1–14
48. Weller RO, Massey A, Newman TA, Hutchings M, Kuo YM, Roher AE (1998) Cerebral amyloid angiopathy: amyloid beta accumulates in putative interstitial fluid drainage pathways in Alzheimer's disease. Am J Pathol 153:725–733
49. White L, Petrovitch H, Hardman J et al (2002) Cerebrovascular pathology and dementia in autopsied Honolulu-Asia Aging Study participants. Ann N Y Acad Sci 977:9–23
50. Wyss-Coray T, Lin C, Yan F et al (2001) TGF-beta1 promotes microglial amyloid-beta clearance and reduces plaque burden in transgenic mice. Nat Med 7:612–618
51. Yamada M, Ihara M, Okamoto Y et al (2011) The influence of chronic cerebral hypoperfusion on cognitive function and amyloid beta metabolism in APP overexpressing mice. PLoS One 6: e16567
52. Yamamoto T, Hirano A (1986) A comparative study of modified Bielschowsky, Bodian and thioflavin S stains on Alzheimer's neurofibrillary tangles. Neuropathol Appl Neurobiol 12:3–9

Experimental Neurology 233 (2012) 523–533

Contents lists available at SciVerse ScienceDirect

Experimental Neurology

journal homepage: www.elsevier.com/locate/yexnr

Cilostazol, a phosphodiesterase inhibitor, prevents no-reflow and hemorrhage in mice with focal cerebral ischemia

Yoshiki Hase, Yoko Okamoto, Youshi Fujita, Akihiro Kitamura, Hitomi Nakabayashi, Hidefumi Ito, Takakuni Maki, Kazuo Washida, Ryosuke Takahashi, Masafumi Ihara *

Department of Neurology, Kyoto University Graduate School of Medicine, Kyoto, Japan

ARTICLE INFO

Article history:
Received 16 August 2011
Revised 5 November 2011
Accepted 25 November 2011
Available online 8 December 2011

Keywords:
Cilostazol
Focal cerebral ischemia
Matrix metalloproteinase
Virchow's triad
Tissue plasminogen activator

ABSTRACT

Background and Purpose: The Cilostazol Stroke Prevention Study II has shown a similar efficacy in stroke prevention but markedly fewer hemorrhagic events with the phosphodiesterase inhibitor cilostazol versus aspirin. The purpose of this study is therefore to investigate how cilostazol affects cerebral hemodynamics and whether it prevents hemorrhagic transformation induced by recombinant tissue plasminogen activator (rtPA) in a mouse model of focal ischemia/reperfusion. Particular emphasis will be placed on the plasma-microvessel interface.

Methods: After receiving food containing 0.3% cilostazol or standard food for 7 days, adult C57BL/6 J mice were subjected to middle cerebral artery occlusion/reperfusion with or without rtPA (10 mg/kg) intravenously administered prior to reperfusion. Cerebral blood flow was monitored at several time points by laser speckle imaging in the 24 hour period post reperfusion, before neurobehavioral and histological assessment. The long-term effect of cilostazol on cerebral ischemia was analyzed in the non-rtPA cohort.

Results: In the non-rtPA cohort, pretreatment by cilostazol significantly decreased the endothelial expression of adhesion molecules (P-selectin and intercellular adhesion molecule-1) and prevented platelet aggregation and leukocyte plugging in the microvessels after cerebral ischemia/reperfusion in the acute phase. Cilostazol significantly reduced mortality rate and improved motor function at 7 days post-ischemia/reperfusion. In the rtPA cohort, cilostazol significantly suppressed edema formation and hemorrhagic transformation with reduced density of microglial cells positive for matrix metalloproteinase-9 in the cerebral cortex and the striatum. In both cohorts, cilostazol significantly suppressed focal no-reflow, mitigated cerebral infarct, and improved neurological outcome.

Conclusions: Cilostazol may possess protective properties against cerebral ischemic injury by preventing no-reflow and hemorrhagic transformation, via maintenance of microvascular integrity.

© 2011 Elsevier Inc. All rights reserved.

Introduction

Virchow's triad has been proposed to describe the vascular basis of ischemic injury in the central nervous system (del Zoppo, 2008). The triad elements consist of injury to vascular endothelium, abnormalities of hemorrheology, and reduction of flow within vascular bed. Their targets are blood vessels, blood elements (i.e., leukocytes, platelets, and coagulation/fibrinolysis system), and blood flow, respectively.

Virchow's multifactorial conceptualization suggests that agents that simultaneously affect more than one element of the triad could be beneficial in reducing the consequences of ischemic injury instead of targeting just one element of the triad. In support of this hypothesis, targeting just one element–inhibition of platelet activation using an αIIbβ3 inhibitor resulted in symptomatic hemorrhage in rodent or nonhuman primate focal ischemia models (Abumiya et al., 2000). Thus, compounds that not only affect platelet function directly, but also indirectly, via action at the vascular wall, may prove useful. For instance, dipyridamole can inhibit platelet aggregation by direct action through a mechanism involving phosphodiesterase-5 but also indirectly by increasing endothelial cell-dependent adenosine concentrations (FitzGerald, 1987). Accordingly, the ESPRIT study indicated that the combination regimen of aspirin plus dipyridamole was superior to aspirin alone as antithrombotic therapy after cerebral ischemia of arterial origin (Halkes et al., 2006).

Another phosphodiesterase inhibitor, cilostazol, acts as an antiplatelet agent and has other pleiotropic effects based on phosphodiesterase-3-dependent mechanisms (Liu et al., 2001). Increasing evidence suggests that cilostazol offers endothelial protection, via an inhibition of

* Corresponding author at: Department of Neurology, Kyoto University Graduate School of Medicine, 54 Kawahara-cho, Shogoin, Sakyo, Kyoto 606–8507 Japan. Fax: +81 75 7514257.

E-mail addresses: hasecchi@kuhp.kyoto-u.ac.jp (Y. Hase), yoko416@kuhp.kyoto-u.ac.jp (Y. Okamoto), fujitauc@kuhp.kyoto-u.ac.jp (Y. Fujita), manto@kuhp.kyoto-u.ac.jp (A. Kitamura), baku@kuhp.kyoto-u.ac.jp (H. Nakabayashi), itohid@kuhp.kyoto-u.ac.jp (H. Ito), harutoma@kuhp.kyoto-u.ac.jp (T. Maki), kazw7@kuhp.kyoto-u.ac.jp (K. Washida), ryosuket@kuhp.kyoto-u.ac.jp (R. Takahashi), ihara@kuhp.kyoto-u.ac.jp (M. Ihara).

0014-4886/$ – see front matter © 2011 Elsevier Inc. All rights reserved.
doi:10.1016/j.expneurol.2011.11.038

apoptosis in endothelial cells (Kim et al., 2002), attenuates the phenotypic modulation of vascular smooth muscle cells (Fujita et al., 2008), and sustains blood flow by endothelium-independent vasodilation (Tanaka et al., 1989). This suggests that cilostazol can affect not only blood elements, such as platelets, but also blood flow and blood vessel integrity, namely all the three elements of Virchow's triad. The recently published Cilostazol Stroke Prevention Study (CSPS)-II showed that cilostazol was, at least, noninferior to aspirin in the prevention of recurrent stroke in patients who had noncardioembolic stroke, and was safer than aspirin; however, cilostazol showed significantly increased side effects, i.e. diarrhea, headache, dizziness, palpitations, as compared to aspirin when used in secondary stroke prevention (Shinohara et al., 2010). Notably, patients taking cilostazol were significantly (54%) less likely to suffer a bleeding event, strengthening the notion that the drug not only has antiplatelet effects but also multifunctional roles that affect more than one target of Virchow's triad with respect to cerebral ischemia.

This study was therefore sought to address the mechanisms behind cilostazol's effect on Virchow's triad and any resultant neurovascular dysfunction after focal ischemia. We therefore assessed whether and, if so, how cilostazol improves the no-reflow phenomenon and how cilostazol prevents recombinant tissue plasminogen activator (rtPA)-induced hemorrhagic transformation in a mouse model of focal ischemia. Particular emphasis was given to the elements of the triad and the plasma-microvessel interface.

Materials and methods

Animals, treatments, and surgical procedures

The experimental protocol is described in Fig. 1. A total of 79 male C57BL/6 J mice (10–12 weeks old, weighing 24–29 g; CLEA Japan, Inc., Tokyo, Japan) were fed with the pelleted food containing 0.3% cilostazol (cilostazol-treated mice, n = 39) or pelleted food only (vehicle-treated mice, n = 40) for 7 days before the operation. All procedures were performed in accordance with the guidelines for animal experimentation from the ethical committee of Kyoto University. The mice were given access to food and water *ad libitum*. We performed middle cerebral artery occlusion/reperfusion (MCAO/R) without blockade of either common carotid artery or pterygopalatine artery blood flow. Detailed surgical procedures of MCAO/R are as follows: Mice were subjected to middle cerebral artery occlusion/reperfusion (MCAO/R) surgery after being anesthetized with 1.5% isoflurane in air. Body temperature was maintained at 37.0 ± 0.5 °C with the aid of feedback warming pad during operation. A midline incision was made in the neck, and the right common carotid artery (CCA), external carotid artery and internal carotid artery were isolated from the vagus nerve. Occipital, superior thyroid, lingual, maxillary arteries, and the external carotid artery were cauterized and cut so that the internal carotid artery and pterygopalatine artery (PPA) were visualized. The stump of the external carotid artery was cut and a filament made of 15 mm of 8–0 nylon string coated with silicon (180–200 μm diameter) was carefully advanced to 11 mm from the carotid artery bifurcation, or until resistance was encountered. We performed MCAO without blockade of either CCA or PPA blood flow (Chen et al., 2008). Approximately 60% reduction of CBF was achieved, as shown previously (Chen et al., 2008). After 45 or 90 minutes of MCAO, the filament was carefully withdrawn to induce vascular re-canalization/reperfusion.

Recombinant tissue plasminogen activator administration

rtPA (10 mg/kg alteplase dissolved with 150 μl of normal saline; Mitsubishi Tanabe Pharma Corporation, Osaka, Japan) was administered through tail vein immediately before reperfusion (45-minute MCAO/R plus rtPA, total n = 12 (cilostazol, n = 6; vehicle, n = 6), 90-minute MCAO/R plus rtPA, total n = 12 (cilostazol, n = 6; vehicle, n = 6)). The dose was in accordance with previous studies (Kollmar et al., 2004).

Measurement of cerebral blood flow

Relative CBF was determined by laser speckle perfusion imaging (Omegazone, Omegawave, Inc., Tokyo, Japan), which obtains high-

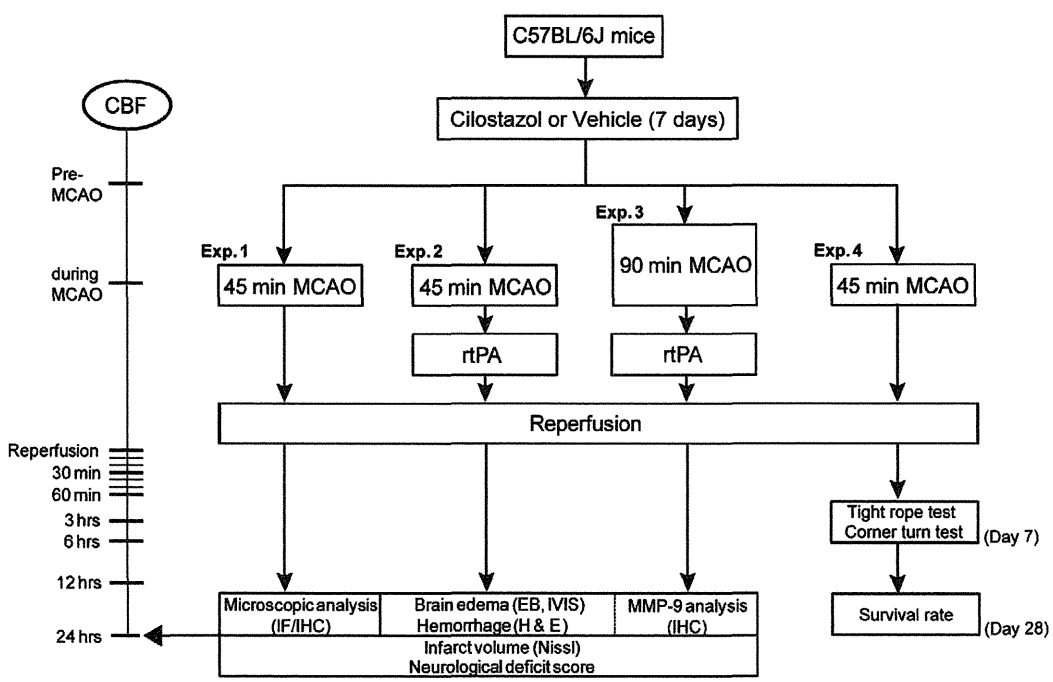

Fig. 1. Experimental protocol. MCAO, middle cerebral artery occlusion; CBF, cerebral blood flow; rtPA, recombinant tissue plasminogen activator; IF, immunofluorescence; IHC, immunohistochemistry; EB, Evans blue; MMP-9, matrix metalloproteinase-9. Exp. 1: total n = 20 (cilostazol, n = 10; vehicle, n = 10). Exp. 2: total n = 12 (cilostazol, n = 6; vehicle, n = 6). Exp. 3: total n = 12 (cilostazol, n = 6; vehicle, n = 6). Exp. 4: total n = 25 (cilostazol, n = 12; vehicle, n = 13).

resolution, two-dimensional imaging and has a linear relationship with absolute CBF values (Fujita et al., 2010). Recordings were performed through the skull under 1.5% isoflurane anesthesia. The periosteum, which adheres to the skull, was widely removed with fine-tip forceps. For each recording, the skull surface was wiped with saline-soaked gauze and then covered with a thin layer of gel (Aquasonic, Parker Laboratories, Inc., Fairfield, NJ) to prevent drying. Calibration was carried out with a calibration reference device (Calibrator S/N 080715-5, Omegawave, Inc., Tokyo, Japan) before each test. The mean CBF was measured in identically sized regions of interest (900 pixels) located 3 mm posterior and 2.5 mm lateral from the bregma. Five recordings of CBF were averaged and CBF values were expressed as a percentage of the preoperative value.

Motor function assessment

Twenty four hours after the surgery, mice (45-minute MCAO/R, total n = 20 (cilostazol, n = 10; vehicle, n = 10), 45-minute MCAO/R plus rtPA, total n = 12 (cilostazol, n = 6; vehicle, n = 6), 90-minute MCAO/R plus rtPA, total n = 10 (cilostazol, n = 5; vehicle, n = 5)) were examined for neurological deficits using a 5-point scale (Chan, 1994). Normal motor function was scored as 0, flexion of the contralateral torso and forelimb on lifting the animal by the tail as 1, circling to the contralateral side but normal posture at rest as 2, leaning to the contralateral side at rest as 3, and no spontaneous motor activity as 4. Scoring was performed by observers blinded to the procedure conducted on the animals. Data were analyzed by analysis of variance, followed by Mann–Whitney U analysis.

Latex perfusion method to assess arterial trunk patency

Mice (45-minute MCAO/R, total n = 10 (cilostazol, n = 5; vehicle, n = 5)) were deeply anesthetized with sodium pentobarbital (50 mg/Kg body weight) and a flexible catheter was inserted from the cardiac apex to the aorta. A mixture of 1 ml carbon black (Bokusai, Osaka, Japan), 10 ml LATEX (Chicago Latex, Crystal Lake, IL), and 10 ml normal saline was prepared and 4 ml infused through a flexible catheter at a constant pressure of 80 mmHg for 60 minutes after the surgery.

FITC-dextran injection to assess microvascular patency

To examine the patency of the cerebral microvessels, mice (45-minute MCAO/R, total n = 10 (cilostazol, n = 5; vehicle, n = 5)) were deeply anesthetized with sodium pentobarbital (50 mg/Kg body weight) and transcardially perfused with 0.1 g of FITC-dextran (2 x 10^6 molecular weight, Sigma, St. Louis, MO) diluted in 7.5 ml of normal saline at the pressure of 120 mmHg. The brains were then removed and fixed in 4% paraformaldehyde (PFA) in 0.1 mol/L PB (pH 7.4). Twenty μm-thick frozen coronal brain sections were made and examined under the fluorescence microscopy (BZ 9000; Keyence, Osaka, Japan).

Evaluation of brain edema and intracerebral hemorrhage

At 24 hours after MCAO/R with rtPA administration, mice (45-minute MCAO/R plus rtPA, total n = 10 (cilostazol, n = 5; vehicle, n = 5), 90-minute MCAO/R plus rtPA, total n = 10 (cilostazol, n = 5; vehicle, n = 5)) were injected with 2% Evans blue dye (Nacalai Tesque, Inc., Kyoto, Japan; diluted in 500 μl of normal saline) intraperitoneally. Two hours later, mice were deeply anesthetized with sodium pentobarbital (50 mg/Kg body weight) and perfused transcardially with normal saline until colorless perfusion fluid was obtained from the right atrium. The brains were then removed and fixed in 4% PFA in 0.1 mol/L PB (pH 7.4). Both the whole brain and 1.0 mm-thick coronally-cut brain sections were analyzed using IVIS® imaging system (Xenogen Caliper Life Sciences, Hopkinton, MA) (605 nm excitation and 680 nm emission) for quantitative analysis of Evans blue extravasation as an estimate of brain edema.

Using the same sections, the volume of intracerebral hemorrhage in every coronal section was calculated by the ABC/2 method (Kothari et al., 1996), as follows (mm^3): the major axis of the hemorrhage (mm) x minor axis of the hemorrhage (mm) x 1 mm (thickness) x 1/2. The volume in each section was then summed to calculate volume of intracerebral hemorrhage in each brain.

The evaluation was performed by an experimenter blind to the animal's group assignment.

Histopathology and immunohistochemistry

Animals were deeply anesthetized with sodium pentobarbital (50 mg/Kg body weight) and purfused transcardially at 20 ml/min with 0.01 mol/L PBS followed by 4% PFA. The brains were dissected out, and the coronally-cut brains were postfixed for 24 hours in 4% PFA in 0.1 mol/L PBS (pH 7.4). Fixed brains were dehydrated and embedded in paraffin. Six μm-thick brain sections were made, and antigen retrieval was performed by the following protocol: 15 minutes boiling in citrate buffer, pH 6.0 for intercellular adhesion molecule-1 (ICAM-1) and P-selectin, or autoclave at 121 °C for 30 minutes in citrate buffer, pH 6.0 for matrix metalloproteinase-9 (MMP-9), or autoclave at 121 °C for 10 minutes in citrate buffer, pH 6.0 for ionized calcium binding adapter molecule-1 (Iba-1). The sections were treated with primary antibodies against ICAM-1 (1:100, R&D systems, Minneapolis, MN), P-selectin (1:50, Santa Cruz Biotechnology, Santa Cruz, CA), MMP-9 (1:50, Santa Cruz) and Iba-1 (1:200, Wako, Osaka, Japan) overnight, followed by incubation with an appropriate secondary antibody (biotinylated anti-IgG; 1:100, Vector Laboratories, Burlingame, CA) for 1 hour and visualization with ABC Kit (Vector Laboratories).

Densitometric analysis for intercellular adhesion molecule-1 (ICAM-1) and P-selectin was carried out after immunohistochemistry (cilostazol, n = 6; vehicle, n = 6). Three different ROIs (0.4 mm^2) were drawn in the penumbral cortex and caudoputamen in close proximity to the lateral ventricle. After images of ICAM-1- and P-selectin-stained sections were captured, ICAM-1- and P-seleectin-positive capillaries were counted in each ROI and averaged.

The numerical density of the Iba-1-positive microglial cells and MMP-9-positive glial cells were counted in the whole cerebral cortex and the striatum of the brain section coronally cut at the bregma. The Iba-1-positive microglial cells with the minimal diameter of their cell bodies exceeding 7 or 10 μm were counted to assess the degree of activation of the microglial cells. The MMP-9-positive glial cells were also counted. After images of MMP-9- and Iba-1-stained sections were captured, areas (mm^2) of the cerebral cortex or striatum were measured by a computerized image system (ImageJ). The density of MMP-9- and Iba-1-positive cells was then calculated per area of the cerebral cortex or the striatum (/mm^2) (90-minute MCAO/R plus rtPA, total n = 12 (cilostazol, n = 6; vehicle, n = 6)).

Immunofluorescent staining

The brains that were fixed in 4% PFA in 0.1 mol/L PB and stored in 20% sucrose in 0.1 mol/L PBS (pH 7.4) after FITC-dextran injection were snap-frozen and 20 μm-thick brain sections were made. The sections were treated with antibodies against ICAM-1 (1:100), P-selectin (1:50), CD45 (1:50, BD Biosciences, San Jose, CA), and CD41 (1:50, BD Biosciences) overnight followed by incubation with rhodamine-conjugated rabbit polyclonal antibody to goat IgG H&L (1:50, Abcam, Cambridge, UK) for CD45 and CD41 or DyLight TM 405-conjugated rabbit polyclonal anti-rat IgG H&L (1:50, ROCKLAND, Gilbertsville, PA) for ICAM-1 and P-selectin. By using paraffin embedded brains, 6 μm-thick coronal brain sections were made, and antigen retrieval

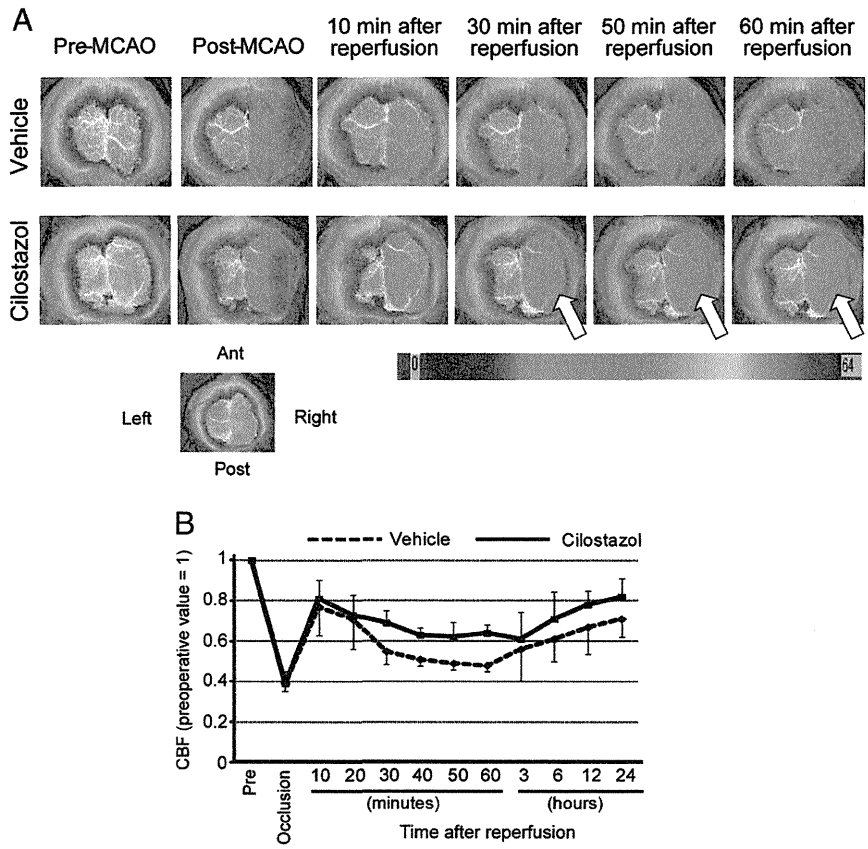

Fig. 2. Cilostazol suppressed no-reflow phenomenon. A, Representative images of cerebral blood flow (CBF) at the indicated time points pre- and post-MCAO/R in vehicle- and cilostazol-treated mice. Arrows indicate suppression of no-reflow phenomenon with cilostazol. B, Temporal profile of CBF of vehicle- and cilostazol-treated mice after 45-minute MCAO/R. CBF was expressed as a ratio to the baseline level (n = 5 each, $P<0.05$).

was performed by autoclave at 121 °C for 30 minutes in citrate buffer, pH 6.0 for MMP-9 and Iba-1. Double immunofluorescent staining was performed using primary antibodies against MMP-9 (1:50, Santa Cruz) and Iba-1 (1:200, Wako) with appropriate fluorescence-labeled secondary antibodies: Alexa Fluor 647 donkey polyclonal anti-goat IgG H&L (1:500, Invitrogen, Carlsbad, CA) for MMP-9 and DyLight TM 488-conjugated donkey polyclonal anti-rabbit IgG H&L (1:400, Jackson Immunoresearch, West Grove, PA) for Iba-1.

Densitometric analysis for microthrombi (CD41) and leukocytes (CD45) in the microvessels was carried out using immunofluorescent staining (cilostazol, n = 6; vehicle, n = 6). Three different ROIs (0.4 mm^2) were drawn in the penumbral cortex and caudoputamen in close proximity to the lateral ventricle. After images of CD41- and CD45-stained sections were captured, the density of CD41-positive microthrombi was measured by a computerized image system (ImageJ) and CD45-positive leukocytes inside the capillaries were counted in each ROI and averaged.

The co-localization ratio of MMP-9 (red) with Iba-1-positive microglia (green) was calculated in the cerebral cortex and caudoputamen at 24 hours after 90-minute MCAO/R plus rtPA (cilostazol, n = 6; vehicle, n = 6). Three different ROIs were drawn in the cerebral cortex and caudoputamen, where MMP-9 was well expressed. Thus, the ratio of MMP-9 positivity among the Iba-1-positive microglia was measured in each ROI and averaged.

Nissl staining

Four serial 2-mm-thick coronal sections between bregma coordinates +2 and −4 were obtained in a cutting block. Each block was embedded in paraffin and 6 μm-thick sections were cut from the caudal side of the block before being subjected to Nissl staining. Images were captured and infarct area was measured (mm^2) in each slice by a computerized image system (ImageJ). The infarction area in each slice x distance between slices (2 mm) were summed to approximate volume of infarct in each brain (mm^3).

Assesment of long-term effect of cilostazol against cerebral ischemia

After 45-minute MCAO/R, mice (total n = 25 (cilostazol, n = 12; vehicle, n = 13)) were observed for 28 days to analyze survival rate. Seven days after the surgery, tight rope (Gerber et al., 2001) and corner turn (Zhang et al., 2002) tests were carried out to analyze any subtle differences in motor coordination (45-minute MCAO/R, total n = 12 (cilostazol, n = 8; vehicle, n = 4)).

Tight rope test: Mice were taken by the tail and placed with their front paws in the middle of a 60 cm-long tight rope about 60 cm above the floor. A box with a padded floor was placed beneath the rope to prevent falling mice being injured. Healthy mice placed on the rope attempted to reach one end of the rope, usually by using

Fig. 3. Cilostazol preserved microvascular patency by suppressing platelet aggregation and leukocyte plugging in microvessels. A and B, Representative fluorescent images of the coronal sections of the brain perfused with FITC-dextran (green) of vehicle- (A) and cilostazol-treated mice (B) after 45-minute MCAO/R. Note the limited perfusion of FITC-dextran in the cortex or the striatum of the vehicle-treated mice (A, arrows). C, Densitometric analysis of the brain perfused with FITC-dextran of vehicle- and cilostazol-treated mice after 45-minute MCAO/R (n = 5 each). D, E, G, and H, Representative images of immunofluorescent staining for CD41 (D and E, red), CD45 (G and H, red), P-selectin (D and E, blue), and ICAM-1 (G and H, blue) of vehicle- (D, G) and cilostazol-treated (E, H) mice. Capillary is visualized with FITC-dextran (D, E, G, and H, green). F and I, Histograms showing the densitometric quantification of the CD41-positive micro-thrombi (F) and CD45-positive leukocytes (I) in the cerebral cortex (Cx) and in the caudoputamen (CP) of the vehicle- and cilostazol-treated mice (n = 5 each). J and K, Densitometric analysis of vessels positive for P-selectin (J) and ICAM-1 (K) (n = 6 each). Scale bars, 1 mm in A and B, 30 μm in D, E, G, and H.

their hind paws and tail for climbing. A tight rope test performance score was given based on whether the animal reached the end of the rope and the time required. A mouse climbing the platform at the side of the rope within 6 s received a score of 0. For each additional 6 s necessary to reach the platform, mice received one additional point. Mice hanging for 60 s at the rope without reaching the platform received a score of 10. Mice that fell from the rope before 60 s received one additional point for each 6 s missing from 60 s (i.e., a mouse unable to stay at the rope received a score of 20); thus, a low score indicated good performance in the tight rope test. All

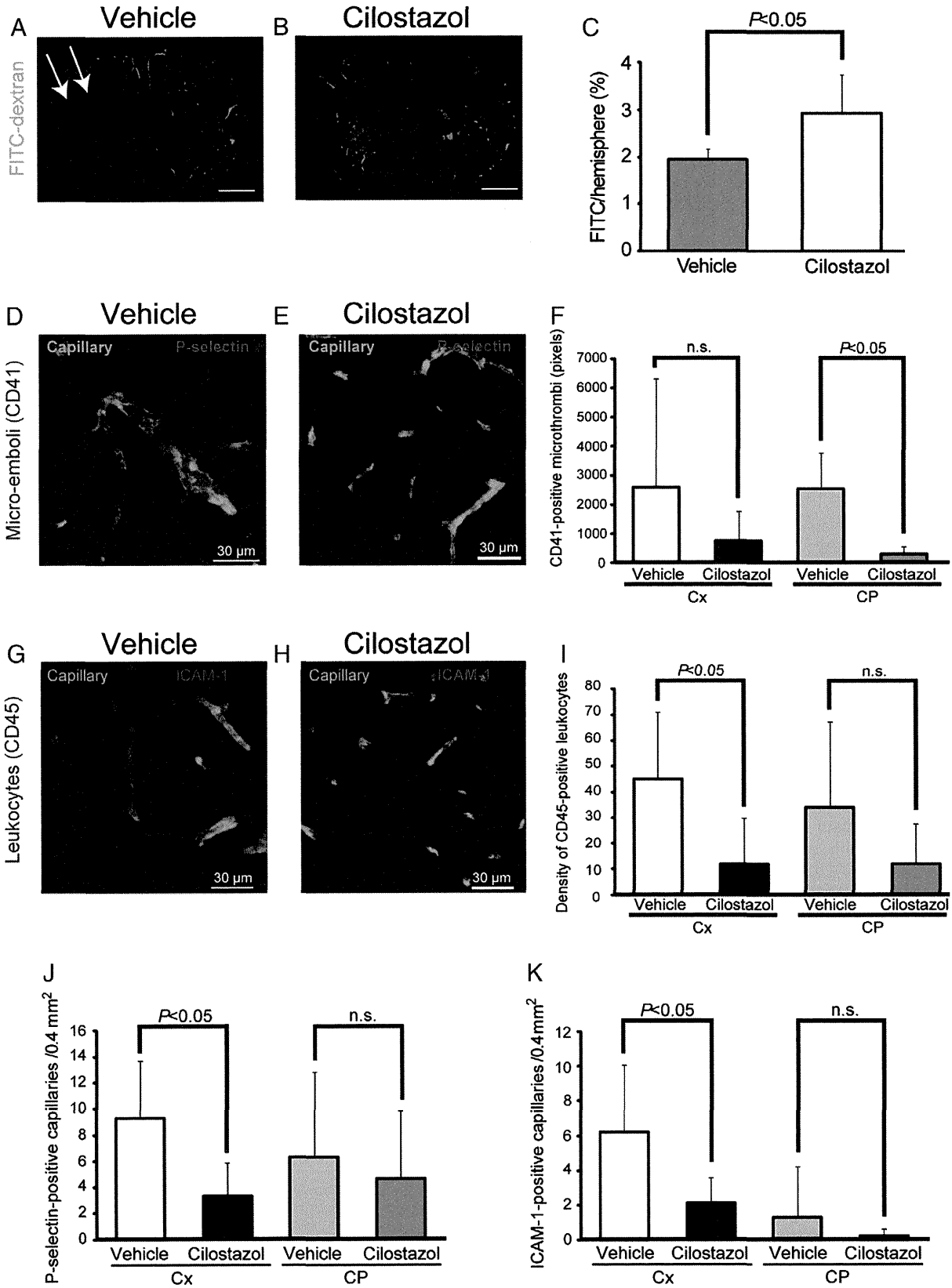

mice were tested twice per time point and their respective scores were used for statistical analysis.

Corner turn test: In the home cage, a mouse was placed between two boards each with dimension of 30 cm x 20 cm x 1 cm. The edges of the two boards were attached at a 30° angle with a small opening along the joint between the two boards to encourage entry into the corner. The mouse was placed between the two angled boards facing the corner and half way to the corner. When entering deep into the corner both sides of the vibrissae were stimulated together. The mouse then rears forward and upward, then turns back to face the open end. The model predicts that the non-ischemic mouse turn either left or right, but the ischemic mouse preferentially turns toward the non-impaired, ipsilateral (right) side. Turning movements that were not part of a rearing movement were not scored. The turns in one versus the other direction were recorded from ten trials for each test and the number of right turns was calculated.

Statistical analysis

All values are expressed as means ± SD in the text and figures. Unpaired *t*-test or one-way ANOVA was used to evaluate significant differences among groups, except where stated, followed by post-hoc Tukey's test or Tukey-Kramer's test. Temporal profiles of CBF were analyzed by two-way repeated measures ANOVA followed by a post-hoc Tukey's test. Differences with $P<0.05$ were considered statistically significant in all analyses.

Results

Mortality rate was less than 10% in the non-rtPA and the rtPA cohort at 24 hours after the surgery

In the non-rtPA cohort, the mortality rate was 9.1% (1 of 11) in vehicle-treated mice and 0% (0 of 10) in cilostazol-treated mice at 24 hours after the surgery. In the rtPA cohort, all of the 24 mice survived until 24 hours after the surgery.

Cilostazol suppressed no-reflow phenomenon in 45-minute MCAO/R

In both vehicle- and cilostazol-treated mice, CBF decreased to approximately 40% of its preoperative level during MCAO (Figs. 2A, B). Ten minutes after reperfusion, CBF recovered to around 80% of its preoperative level. However, beginning at 20 minutes after reperfusion, CBF gradually decreased despite vascular recanalization in vehicle-treated mice (n = 5), indicative of no-reflow phenomenon. In cilostazol-treated mice, the no-reflow phenomenon was significantly suppressed; the degree of CBF reduction was also less apparent during the 60 minute period after reperfusion. CBF began to recover at 3 hours after reperfusion and continued at least until 24 hours after reperfusion. The CBF recovery was significantly greater in the cilostazol-treated group ($P<0.05$). CBF recovered to approximately 80% of its preoperative level in the cilostazol-treated mice, but to 70% in vehicle-treated mice at 24 hours after reperfusion.

Cilostazol preserved microvascular blood flow in ischemic area by preventing microvascular obstruction by leukocytes and microthrombi in 45-minute MCAO/R

Latex perfusion analyses showed that the main MCA trunk was patent both in the vehicle- and cilostazol-treated mice, after MCAO/R. Therefore, the cilostazol-induced suppression of the no-reflow phenomenon is not considered to be linked to occlusion or stenosis of the main trunk of MCA; this therefore led us to focus on plasma-microvessel interface. In vehicle-treated mice, capillaries in ischemic regions were not sufficiently perfused with FITC-dextran with perfusion pressure reaching 120 mmHg. In cilostazol-treated mice, however, a greater number of capillaries were filled with FITC-dextran (Figs. 3A–C). Cilostazol-treated mice exhibited less capillary micro-thrombi formation in the striatum (Figs. 3D–F) and fewer lodged leukocytes in the capillaries of the cerebral cortex (Figs. 3G–I). Moreover, cilostazol-treated mice exhibited less expression of endothelial adhesion molecules, such as intercellular adhesion molecule-1 (ICAM-1) and P-selectin, in the ischemic cerebral cortex (Figs. 3J, K).

Cilostazol reduced infarct volume and improved motor function after 45-minute MCAO/R

Cilostazol-treated mice showed significantly less infarct volume (Figs. 4A–C) and better motor function (Fig. 4D).

Cilostazol promoted faster CBF recovery after 45-minute MCAO/R plus rtPA

After 45-minute MCAO/R plus rtPA, CBF decreased to approximately 40% of its preoperative level during MCAO in both vehicle and cilostazol-treated mice. At 10 minutes after reperfusion, CBF recovered to approximately 70% of its preoperative level in cilostazol-treated mice, but remained below 60% in vehicle-treated mice (Fig. 6A). Beginning at 20 minutes, CBF gradually decreased despite vascular recanalization at least until 1 hour after reperfusion. However, cilostazol-treated mice exhibited slightly increased CBF during this period. At 3 hours after reperfusion, the downward trend was reversed, with cilostazol-treated mice showing faster CBF recovery. Cilostazol-treated mice showed significantly better recovery of CBF ($P<0.05$).

Cilostazol ameliorated brain edema and hemorrhagic transformation after 45- or 90-minute MCAO/R plus rtPA

Using the IVIS® imaging system, whole brain analysis of extravasated Evans blue dye was conducted. Cilostazol-treated mice showed a nonsignificant trend toward less rtPA-induced brain

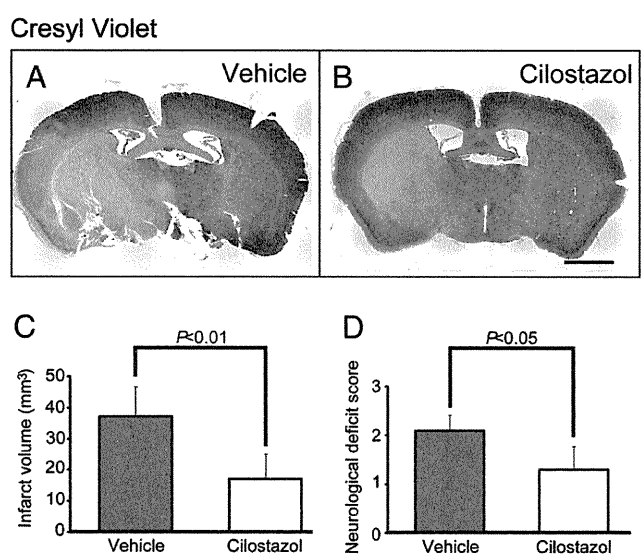

Fig. 4. Cilostazol reduced infarct volume and ameliorated neurological deficits. A and B, Representative images of Nissl staining of the brain of vehicle-treated (A) and cilostazol-treated (B) mice after 45-minute MCAO/R. C and D, Histograms showing the infarct volume (mm^3) (C) (cilostazol, n = 6; vehicle, n = 9) and the neurological deficit score (D) (n = 10 each) of the vehicle- or cilostazol-treated mice at 24 hours after 45-minute MCAO/R. Scale bars, 1 mm.

edema after 45-minute MCAO/R and significantly less brain edema after 90-minute MCAO/R (Figs. 5A–C). rtPA administration induced intracerebral hemorrhage in most of the vehicle-treated mice after 45-minute (in 4 out of 5 mice) and 90-minute (in all 5 mice) MCAO/R. Cilostazol almost completely prevented the hemorrhagic transformation and significantly reduced the volume of rtPA-induced hemorrhage in both cohorts (Figs. 5D–F).

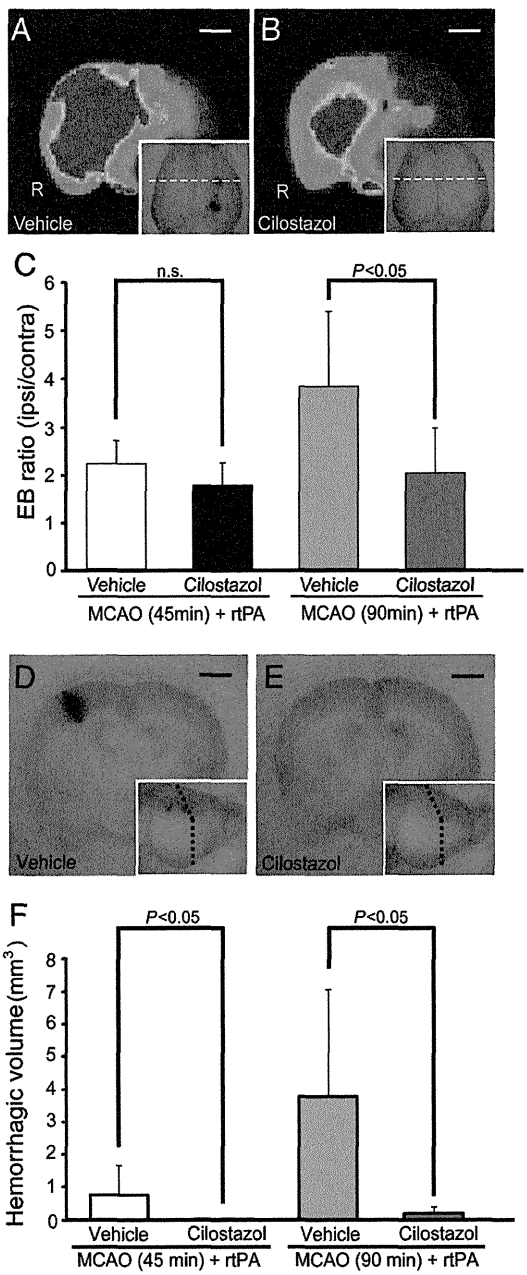

Fig. 5. Cilostazol reduced rtPA-induced brain edema and hemorrhagic transformation. A and B, Representative IVIS® images of coronal brain sections of vehicle-treated (A) and cilostazol-treated (B) mice injected with Evans blue at 24 hours after 90-minute MCAO/R plus rtPA. Insets show representative dorsal view of the brain. C, Histogram showing ipsilateral-to-contralateral ratio of Evans blue extravasation of vehicle-treated and cilostazol-treated mice at 24 hours after 45-minute (n = 5 each) or 90-minute (n = 5 each) MCAO/R plus rtPA. D and E, Representative images of coronal brain sections of vehicle-treated (D) and cilostazol-treated (E) mice at 24 hours after 90-minute MCAO/R plus rtPA. Insets show representative laterodorsal view of the brain. F, Histogram showing hemorrhagic volume of vehicle-treated and cilostazol-treated mice at 24 hours after 45-minute (n = 5 each) or 90-minute (n = 5 each) MCAO/R plus rtPA. Scale bars, 1 mm.

Cilostazol suppressed microglial activation and MMP-9 expression in the microglia

After 90-minute MCAO/R plus rtPA, activated microglial cells expressed matrix metalloproteinase-9 (MMP-9) in ischemic areas of both the cerebral cortex and caudoputamen in vehicle-treated mice (Figs. 6B, D). Cilostazol significantly attenuated such microglial activation (Figs. 6C, G, and H) and MMP-9 expression compared to vehicle-treated mice (Figs. 6E, F).

Cilostazol reduced infarct volume and improved motor function after 45- or 90-minute MCAO/R with rtPA administration

Cilostazol-treated mice showed significantly less infarct volume (Figs. 7A–E) and better motor function at 24 hours after 45- or 90-minute MCAO/R plus rtPA (Fig. 7F).

Cilostazol reduced a mortality rate during the 28-day period after 45-minute MCAO/R

In vehicle-treated mice, the mortality rate was 69% (9 of 13) at 7 days, and 85% (11 of 13) at 28 days after 45-minute MCAO/R. However, in cilostazol-treated mice, the mortality rate was 25% (3 of 12) at 7 days, and 33% (4 of 12) at 28 days after surgery. Cilostazol significantly reduced a mortality rate until 28 days after 45-minute MCAO/R (Kaplan-Meier survival analysis, log-rank $P<0.01$) (Fig. 8A).

Cilostazol improved motor function at 7 days after 45-minute MCAO/R

The performance in the tight rope test was significantly improved in cilostazol-treated mice compared to vehicle-treated mice at 7 days after 45-minute MCAO/R (Fig. 8B). In the corner turn test, cilostazol-treated mice showed a significant decrease in the right turns compared to vehicle-treated mice at 7 days after 45-minute MCAO/R (Fig. 8C).

Discussion

This study using a mouse model of focal cerebral ischemia showed that cilostazol: (1) preserved microvascular patency by decreasing the endothelial expression of P-selectin and ICAM-1 and therefore prevented platelet aggregation and leukocyte plugging in microvessels in the acute phase in the non-rtPA cohort, which subsequently lead to a reduced mortality rate and improved motor function in a later phase; (2) ameliorated rtPA-induced brain edema and hemorrhagic transformation at least partially due to suppression of microglial MMP-9 expression in the rtPA cohort; (3) suppressed focal no-reflow, mitigated cerebral infarct, and improved neurological outcome in both cohorts. Such pleiotropic effects of cilostazol, that are at least partially exerted by vascular protection, may explain the effectiveness of CSPS (Gotoh et al., 2000), CASISP (Huang et al., 2008), and CSPS-II (Shinohara et al., 2010).

Early restoration of antegrade flow is expected to enhance the functional recovery after stroke. However, recent studies have demonstrated that successful reopening of an occluded artery with rtPA does not necessarily lead to clinical improvement (Alexandrov et al., 2004); such phenomenon is explained by several potential mechanisms, including edema formation (von Kummer et al., 2001), hemorrhagic transformation (Alexandrov and Grotta, 2002), no-reflow phenomenon (del Zoppo and Hallenbeck, 2000), proximal reocclusion (Alexandrov and Grotta, 2002), and reperfusion injury (Uematsu et al., 1989). Such predisposing factors warrant treatment as delayed recovery of brain function may still occur in these patients with 'ischemic stunning of the brain' (Alexandrov et al., 2004). Such predisposing factors may be closely linked with the three elements of the Virchow's triad: 1) blood vessels are linked with edema/

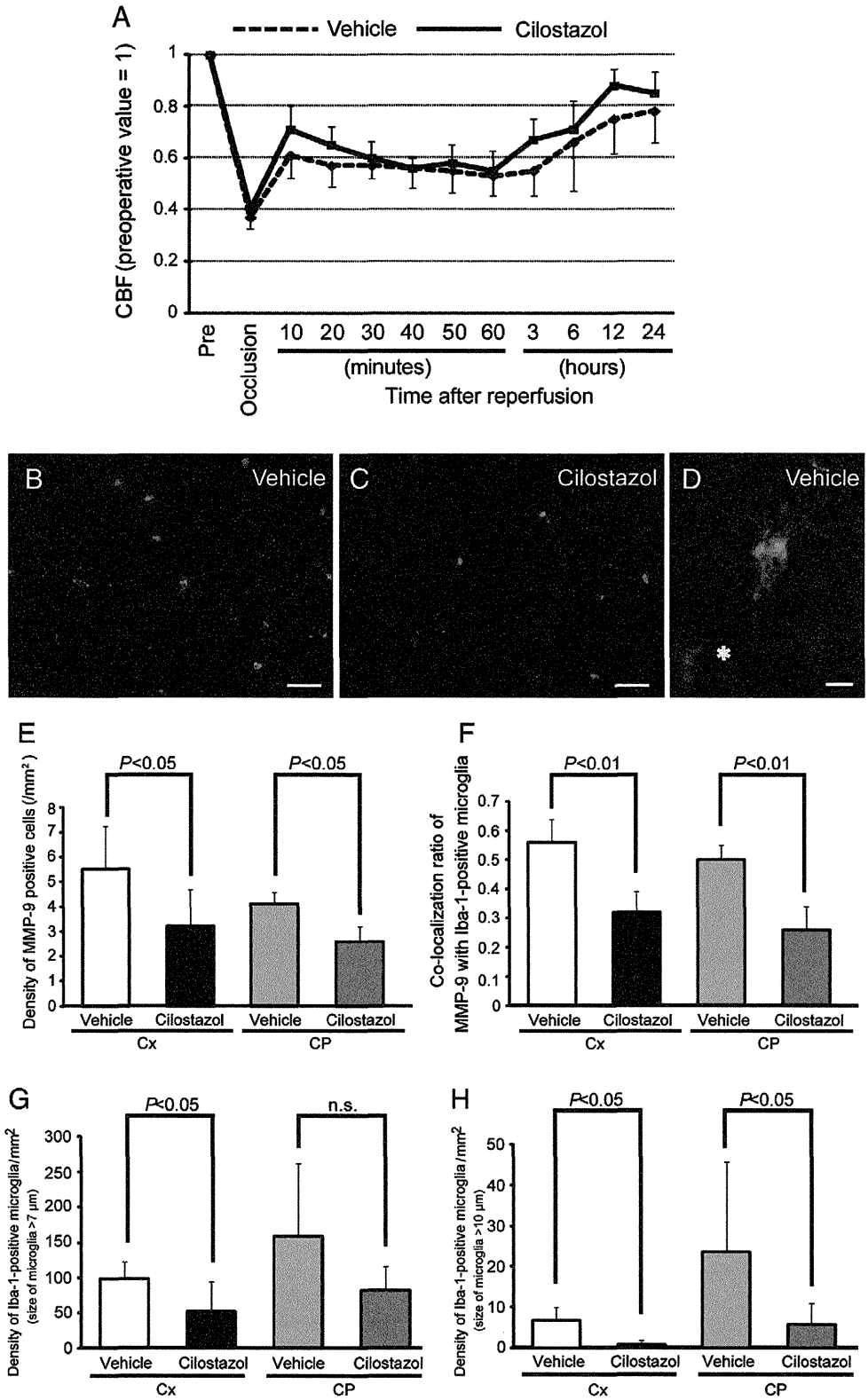

Fig. 6. Cilostazol promoted faster recovery of cerebral blood flow and reduced MMP-9 positive activated microglia after MCAO/R plus rtPA. A, Temporal profile of cerebral blood flow (CBF) of vehicle- and cilostazol-treated mice after 45-minute MCAO/R plus rtPA (n = 5 each, $P<0.05$). The preoperative CBF value was set as 1. B–D, Representative images of immunofluorescent staining for MMP-9 (red) and Iba-1-positive microglia (green) in ischemic cortical hemisphere of vehicle-treated (B, D) and cilostazol-treated (C) mice at 24 hours after 90-minute MCAO/R plus rtPA. An enlarged microglial cell with thickened processes secretes MMP-9 around a vessel (D, asterisk). Nuclei are stained with DAPI (D, blue). E and F, Histograms showing the density of MMP-9-positive cells per mm^2 (E) and co-localization ratio of MMP-9 with Iba-1-positive microglial cells (F) in the cerebral cortex (Cx) and the caudoputamen (CP) of the vehicle-treated and cilostazol-treated mice at 24 hours after 90-minute MCAO/R plus rtPA (n = 6 each). G and H, Histograms showing the density (/mm^2) of 'activated' microglia, with a cell body size exceeding 7 μm (G) and 'highly activated' microglia, with a cell body size exceeding 10 μm (H) in the ischemic cerebral cortex (Cx) and caudoputamen (CP) of the vehicle- or cilostazol-treated mice after 90-minute MCAO/R plus rtPA (n = 6 each). Scale bars, 40 μm (B, C), 10 μm (D).

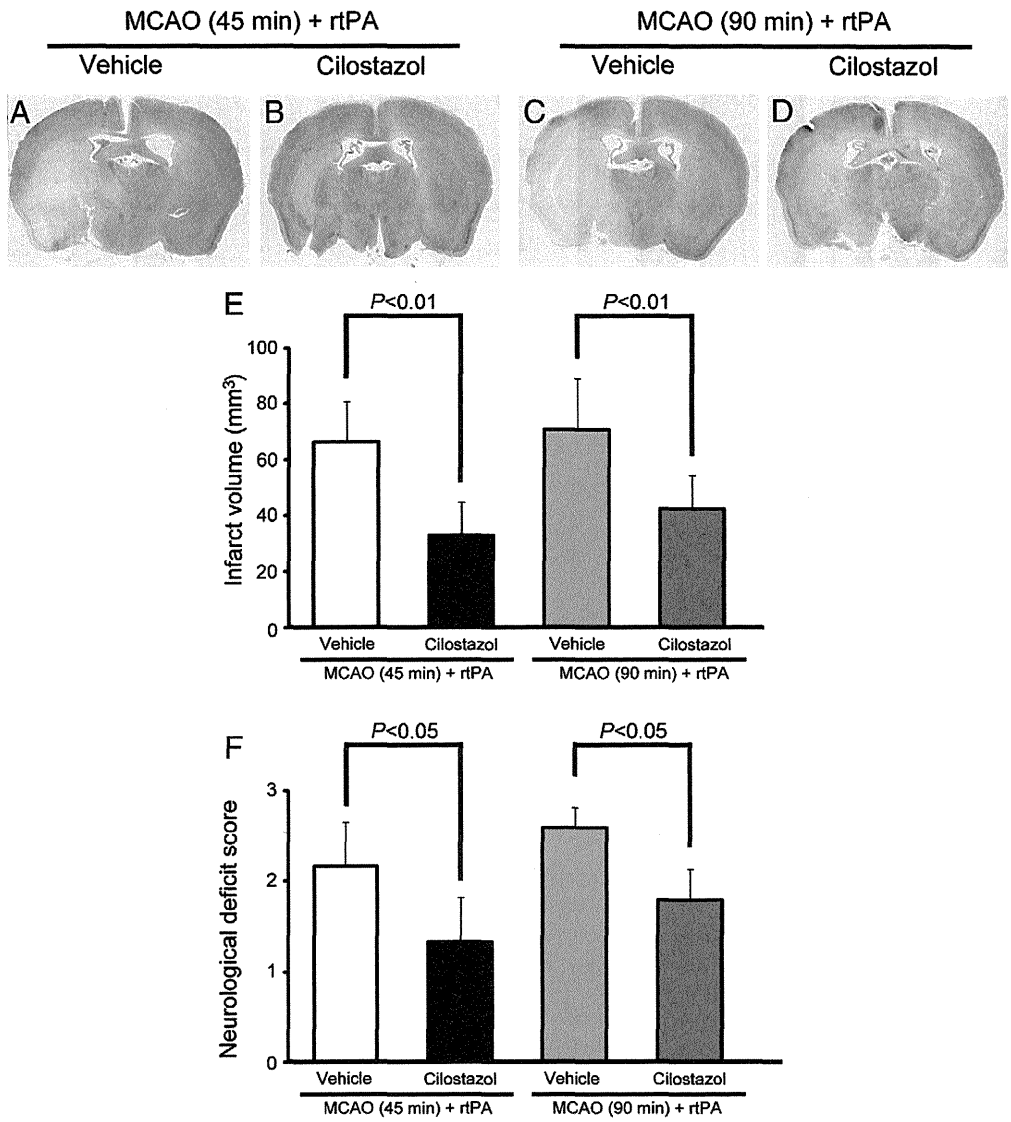

Fig. 7. Cilostazol reduced infarct volume and ameliorated neurological deficits after MCAO/R plus rtPA. A–D, Representative images of Nissl staining of the coronally-cut brain of the vehicle-treated (A, C) or cilostazol-treated (B, D) mice at 24 hours after 45-minute (A, B) or 90-minute (C, D) MCAO/R in combination with rtPA. E and F, Histograms showing the infarct volume (mm^3) (E) (45-minute MCAO/R plus rtPA, n = 5 each; 90-minute MCAO/R plus rtPA, n = 5 each) and the neurological deficit score (F) (45-minute MCAO/R plus rtPA, n = 6 each; 90-minute MCAO/R plus rtPA, n = 5 each) of the vehicle- or cilostazol-treated mice at 24 hours after 45-minute or 90-minute MCAO/R plus rtPA.

hemorrhage formation or reperfusion injury; 2) blood flow is associated with no-reflow phenomenon; and 3) blood elements are associated with proximal reocclusion. Therefore, these three elements would be a suitable starting point when considering a combination therapy with rtPA. In addition, platelet hyperaggregability may ensue after rtPA therapy (Ohlstein et al., 1987), providing a rationale of using antiplatelet drug such as cilostazol to salvage ischemic stunning of the brain after rtPA therapy.

Several studies have reported the neuroprotective roles of cilostazol in acute brain injury in experimental rodent models of MCAO/R. Following 2-hour MCAO/R in Sprague–Dawley rats, post-ischemic administration of cilostazol resulted in reduction of infarct volume with reduced apoptosis and upregulated bcl-2 (Choi et al., 2002; Lee et al., 2004). Another study showed cilostazol, given immediately after 45-min MCAO/R, mitigated infarction and enhanced neurogenesis in C57BL/6 mice (Tanaka et al., 2010). This protection was achieved by a cAMP response-element-binding protein-mediated signaling pathway, without CBF changes at 1, 3, and 7 days after reperfusion (Tanaka et al., 2010). Thus, cilostazol may protect against ischemic neuronal damage through its cAMP-elevating activity even without CBF changes. However, since the above studies did not evaluate CBF within 1 day after reperfusion, there is still a possibility that cilostazol exerted a neuroprotective role by restoring CBF in an earlier phase after reperfusion. By monitoring CBF in the 24 hours, our study showed that cilostazol suppressed the no-reflow phenomenon by restoring microvascular circulation at an earlier phase. In accordance with this result, in a different experimental paradigm using photothrombotic permanent MCAO in spontaneously hypertensive rats, cilostazol given 2 hours before or 30 min after MCAO significantly reduced infarct volume; this was accompanied by increased CBF at 1- and 2-hour post-MCAO (Ito et al., 2010).

A recent study has reported that cilostazol prevented rtPA-induced hemorrhagic transformation, brain edema, and endothelial injury at 18 hours after reperfusion in ddY mice with 6-hour MCAO/R (Ishiguro et al., 2010). Although CBF was not examined in the previous study, the notable effects of cilostazol were explained by reduced MMP-9 activity and restored claudin-5 expression. This is consistent with our results, which showed that cilostazol may protect the blood–brain barrier (BBB) by downregulating the microglial MMP-9

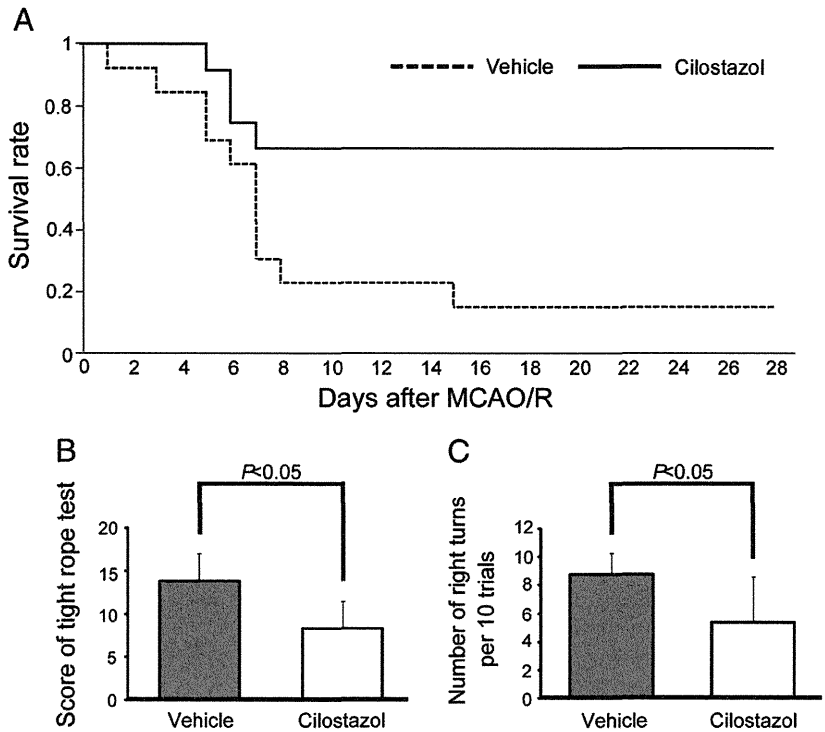

Fig. 8. Cilostazol reduced a mortality rate and improved motor function. A, Kaplan-Meier survival analysis after 45-minute MCAO/R, showing that cilostazol significantly reduced a mortality rate during the following 28 days (cilostazol, n = 12; vehicle, n = 13; log-rank $P<0.01$). B and C, Histograms showing the score of the tight rope test (B) and the number of right turns in the corner turn test (C) at 7 days after 45-minute MCAO/R (cilostazol, n = 8; vehicle, n = 4).

expression. Alternatively, cilostazol may have a direct protective effect on vasculature given the absence of any difference in brain edema but the presence of significant difference in hemorrhagic volume between vehicle- and cilostazol-treated groups after 45-minute MCAO/R plus rtPA.

Previous reports indicate that cerebral ischemia activates MCP-1 production via NF-κB signaling pathway (Liu et al., 2001) or activates mitogen-activated protein kinases (Maddahi et al., 2009), both leading to MMP-9 activation. rtPA is also known to increase MMP-9 through induction of low-density lipoprotein receptor-related protein (Wang et al., 2003). Given that cAMP suppresses NF-κB, MCP-1, and mitogen-activated protein kinases (Tsai et al., 2008), cilostazol may prevent BBB leakage via MMP-9 inhibition. Thus, besides its antiplatelet activity, cilostazol has a role in restoring CBF and protecting endothelial function, making it a candidate drug for a combination therapy with rtPA.

The long-term effects of cilostazol warrant further investigation using a focal ischemia model of 45-minute MCAO/R. Previous reports indicate that a mortality rate at 7 days is more than 50% after 60-minute MCAO/R (Komine-Kobayashi et al., 2004) and 100% after 6-hour MCAO/R (Ishiguro et al., 2010). As expected, in vehicle-treated mice, a mortality rate was high, measuring 69% at 7 days, and 85% at 28 days after 45-minute MCAO/R, in accordance with the previous report (Komine-Kobayashi et al., 2004). However, in cilostazol-treated mice, the mortality rate was 25% at 7 days, and 33% at 28 days after the surgery. Cilostazol significantly reduced the mortality rate during 28 days after 45-minute MCAO/R; this could thus be deduced as a neuroprotective effect of cilostazol. Because a high mortality rate was anticipated after 45-minute MCAO/R, neurobehavioral assessment was carried out at 7 days after the surgery. Cilostazol-treated mice showed significantly better performance in the tight rope test and the corner turn test although confounded by a survival bias. Thus, long-term effect of cilostazol against ischemic stroke was demonstrated.

A limitation of this study is that cilostazol was administered prior to induction of MCAO/R to obtain its stable blood concentration. However, cilostazol is known to show maximal plasma levels at 2 to 4 hours after oral administration in rats, and pre-ischemic and post-ischemic administration of cilostazol were almost equally effective to mitigate infarction in permanent MCAO model (Ito et al., 2010). Therefore, post-ischemic administration of cilostazol might be also effective against no-reflow phenomenon in transient focal ischemia. If extrapolated clinically, the current study suggests that cilostazol could be a promising drug for secondary prevention of stroke by minimizing focal brain ischemia and rtPA-induced BBB leakage in preparation for any subsequent stroke. In acute clinical settings, however, it remains to be elucidated whether post-ischemic administration of cilostazol, with or without concomitant rtPA, ameliorates the no-reflow phenomenon.

In conclusion, cilostazol can be considered a safe and beneficial vasculo- and neuroprotective agent that affects different components of the ischemic cascade and enhances the therapeutic effects of thrombolysis by restoring the integrity of the plasma-vessel interface.

Source of funding

This work was supported by a Grant-in-Aid for Exploratory Research from the Japanese Ministry of Education, Culture, Sports, Science and Technology (M.I., No. 22650073), and by the Research fund from the Otsuka Pharmaceutical Co. Ltd. (Tokyo, Japan).

Disclosures

The study is designed, conducted, analyzed, and reported independently of the funding agencies and pharmaceutical companies, although cilostazol was supplied by Otsuka Pharmaceutical Co. Ltd. and alteplase by Mitsubishi Tanabe Pharma Corporation (Osaka, Japan).

Acknowledgment

The authors are grateful to Dr. Ahmad Khundakar for his insightful comments. We also thank Ms. Takako Kawada for assistance in staining the tissue sections.

References

Abumiya, T., Fitridge, R., Mazur, C., Copeland, B.R., Koziol, J.A., Tschopp, J.F., Pierschbacher, M.D., del Zoppo, G.J., 2000. Integrin alpha(IIb)beta(3) inhibitor preserves microvascular patency in experimental acute focal cerebral ischemia. Stroke 31, 1402–1409 discussion 1409–1410.

Alexandrov, A.V., Grotta, J.C., 2002. Arterial reocclusion in stroke patients treated with intravenous tissue plasminogen activator. Neurology 59, 862–867.

Alexandrov, A.V., Hall, C.E., Labiche, L.A., Wojner, A.W., Grotta, J.C., 2004. Ischemic stunning of the brain: early recanalization without immediate clinical improvement in acute ischemic stroke. Stroke 35, 449–452.

Chan, P.H., 1994. Oxygen radicals in focal cerebral ischemia. Brain Pathol. 4, 59–65.

Chen, Y., Ito, A., Takai, K., Saito, N., 2008. Blocking pterygopalatine arterial blood flow decreases infarct volume variability in a mouse model of intraluminal suture middle cerebral artery occlusion. J. Neurosci. Methods 174, 18–24.

Choi, J.M., Shin, H.K., Kim, K.Y., Lee, J.H., Hong, K.W., 2002. Neuroprotective effect of cilostazol against focal cerebral ischemia via antiapoptotic action in rats. J. Pharmacol. Exp. Ther. 300, 787–793.

del Zoppo, G.J., 2008. Virchow's triad: the vascular basis of cerebral injury. Rev. Neurol. Dis. 5 (Suppl. 1), S12–S21.

del Zoppo, G.J., Hallenbeck, J.M., 2000. Advances in the vascular pathophysiology of ischemic stroke. Thromb. Res. 98, 73–81.

FitzGerald, G.A., 1987. Dipyridamole. N. Engl. J. Med. 316, 1247–1257.

Fujita, Y., Lin, J.X., Takahashi, R., Tomimoto, H., 2008. Cilostazol alleviates cerebral small-vessel pathology and white-matter lesions in stroke-prone spontaneously hypertensive rats. Brain Res. 1203, 170–176.

Fujita, Y., Ihara, M., Ushiki, T., Hirai, H., Kizaka-Kondoh, S., Hiraoka, M., Ito, H., Takahashi, R., 2010. Early protective effect of bone marrow mononuclear cells against ischemic white matter damage through augmentation of cerebral blood flow. Stroke 41, 2938–2943.

Gerber, J., Raivich, G., Wellmer, A., Noeske, C., Kunst, T., Werner, A., Bruck, W., Nau, R., 2001. A mouse model of Streptococcus pneumoniae meningitis mimicking several features of human disease. Acta Neuropathol. 101, 499–508.

Gotoh, F., Tohgi, H., Hirai, S., Terashi, A., Fukuuchi, Y., Otomo, E., Shinohara, Y., Itoh, E., Matsuda, T., Sawada, T., Yamaguchi, T., Nishimaru, K., Ohashi, Y., 2000. Cilostazol stroke prevention study: A placebo-controlled double-blind trial for secondary prevention of cerebral infarction. J. Stroke Cerebrovasc. Dis. 9, 147–157.

Halkes, P.H., van Gijn, J., Kappelle, L.J., Koudstaal, P.J., Algra, A., 2006. Aspirin plus dipyridamole versus aspirin alone after cerebral ischaemia of arterial origin (ESPRIT): randomised controlled trial. Lancet 367, 1665–1673.

Huang, Y., Cheng, Y., Wu, J., Li, Y., Xu, E., Hong, Z., Li, Z., Zhang, W., Ding, M., Gao, X., Fan, D., Zeng, J., Wong, K., Lu, C., Xiao, J., Yao, C., 2008. Cilostazol as an alternative to aspirin after ischaemic stroke: a randomised, double-blind, pilot study. Lancet Neurol. 7, 494–499.

Ishiguro, M., Mishiro, K., Fujiwara, Y., Chen, H., Izuta, H., Tsuruma, K., Shimazawa, M., Yoshimura, S., Satoh, M., Iwama, T., Hara, H., 2010. Phosphodiesterase-III inhibitor prevents hemorrhagic transformation induced by focal cerebral ischemia in mice treated with tPA. PLoS One 5, e15178.

Ito, H., Hashimoto, A., Matsumoto, Y., Yao, H., Miyakoda, G., 2010. Cilostazol, a phosphodiesterase inhibitor, attenuates photothrombotic focal ischemic brain injury in hypertensive rats. J. Cereb. Blood Flow Metab. 30, 343–351.

Kim, K.Y., Shin, H.K., Choi, J.M., Hong, K.W., 2002. Inhibition of lipopolysaccharide-induced apoptosis by cilostazol in human umbilical vein endothelial cells. J. Pharmacol. Exp. Ther. 300, 709–715.

Kollmar, R., Henninger, N., Bardutzky, J., Schellinger, P.D., Schabitz, W.R., Schwab, S., 2004. Combination therapy of moderate hypothermia and thrombolysis in experimental thromboembolic stroke–an MRI study. Exp. Neurol. 190, 204–212.

Komine-Kobayashi, M., Chou, N., Mochizuki, H., Nakao, A., Mizuno, Y., Urabe, T., 2004. Dual role of Fcgamma receptor in transient focal cerebral ischemia in mice. Stroke 35, 958–963.

Kothari, R.U., Brott, T., Broderick, J.P., Barsan, W.G., Sauerbeck, L.R., Zuccarello, M., Khoury, J., 1996. The ABCs of measuring intracerebral hemorrhage volumes. Stroke 27, 1304–1305.

Lee, J.H., Kim, K.Y., Lee, Y.K., Park, S.Y., Kim, C.D., Lee, W.S., Rhim, B.Y., Hong, K.W., 2004. Cilostazol prevents focal cerebral ischemic injury by enhancing casein kinase 2 phosphorylation and suppression of phosphatase and tensin homolog deleted from chromosome 10 phosphorylation in rats. J. Pharmacol. Exp. Ther. 308, 896–903.

Liu, Y., Shakur, Y., Yoshitake, M., Kambayashi Ji, J., 2001. Cilostazol (pletal): a dual inhibitor of cyclic nucleotide phosphodiesterase type 3 and adenosine uptake. Cardiovasc. Drug Rev. 19, 369–386.

Maddahi, A., Chen, Q., Edvinsson, L., 2009. Enhanced cerebrovascular expression of matrix metalloproteinase-9 and tissue inhibitor of metalloproteinase-1 via the MEK/ERK pathway during cerebral ischemia in the rat. BMC Neurosci. 10, 56.

Ohlstein, E.H., Storer, B., Fujita, T., Shebuski, R.J., 1987. Tissue-type plasminogen activator and streptokinase induce platelet hyperaggregability in the rabbit. Thromb. Res. 46, 575–585.

Shinohara, Y., Katayama, Y., Uchiyama, S., Yamaguchi, T., Handa, S., Matsuoka, K., Ohashi, Y., Tanahashi, N., Yamamoto, H., Genka, C., Kitagawa, Y., Kusuoka, H., Nishimaru, K., Tsushima, M., Koretsune, Y., Sawada, T., Hamada, C., 2010. Cilostazol for prevention of secondary stroke (CSPS 2): an aspirin-controlled, double-blind, randomised non-inferiority trial. Lancet Neurol. 9, 959–968.

Tanaka, K., Gotoh, F., Fukuuchi, Y., Amano, T., Uematsu, D., Kawamura, J., Yamawaki, T., Itoh, N., Obara, K., Muramatsu, K., 1989. Effects of a selective inhibitor of cyclic AMP phosphodiesterase on the pial microcirculation in feline cerebral ischemia. Stroke 20, 668–673.

Tanaka, Y., Tanaka, R., Liu, M., Hattori, N., Urabe, T., 2010. Cilostazol attenuates ischemic brain injury and enhances neurogenesis in the subventricular zone of adult mice after transient focal cerebral ischemia. Neuroscience 171, 1367–1376.

Tsai, C.S., Lin, F.Y., Chen, Y.H., Yang, T.L., Wang, H.J., Huang, G.S., Lin, C.Y., Tsai, Y.T., Lin, S.J., Li, C.Y., 2008. Cilostazol attenuates MCP-1 and MMP-9 expression in vivo in LPS-administrated balloon-injured rabbit aorta and in vitro in LPS-treated monocytic THP-1 cells. J. Cell. Biochem. 103, 54–66.

Uematsu, D., Greenberg, J.H., Reivich, M., Hickey, W.F., 1989. Direct evidence for calcium-induced ischemic and reperfusion injury. Ann. Neurol. 26, 280–283.

von Kummer, R., Bourquain, H., Bastianello, S., Bozzao, L., Manelfe, C., Meier, D., Hacke, W., 2001. Early prediction of irreversible brain damage after ischemic stroke at CT. Radiology 219, 95–100.

Wang, X., Lee, S.R., Arai, K., Tsuji, K., Rebeck, G.W., Lo, E.H., 2003. Lipoprotein receptor-mediated induction of matrix metalloproteinase by tissue plasminogen activator. Nat. Med. 9, 1313–1317.

Zhang, L., Schallert, T., Zhang, Z.G., Jiang, Q., Arniego, P., Li, Q., Lu, M., Chopp, M., 2002. A test for detecting long-term sensorimotor dysfunction in the mouse after focal cerebral ischemia. J. Neurosci. Methods 117, 207–214.